2012

Computational Investigation of Drag Reduction with a Rear Flap on Trucks

Yangyang Hu
University of Alabama at Birmingham

COMPUTATIONAL INVESTIGATION OF DRAG REDUCTION WITH A REAR FLAP ON TRUCKS

by

YANGYANG HU

ALAN SHIH, COMMITTEE CHAIR
JONG-EUN KIM
ROY KOOMULLIL

A THESIS

Submitted to the graduate faculty of The University of Alabama at Birmingham,
in partial fulfillment of the requirements for the degree of
Master of Science in Mechanical Engineering

BIRMINGHAM, ALABAMA

2012

COMPUTATIONAL INVESTIGATION OF DRAG REDUCTION WITH A REAR FLAP ON TRUCKS

YANGYANG HU

DEGREE: MS PROGRAM: MECHANICAL ENGINEERING

ABSTRACT

Computational fluid dynamic (CFD) simulations of the steady state Reynolds-Averaged Navier-Stokes (RANS) equations using the second order $k-\omega$ turbulence model were performed to investigate the Drag Coefficients (C_d) of the Class 8 trucks under different geometric configurations. The reduction rates of aerodynamic drag using several add-on devices such as base flap, boat tail, underbody skirt, and tractor-trailer gap are investigated through the CFD simulations. Moreover, simulations by using different lengths and angles of the base flap and boat tail were conducted; the comparison indicates that the base flap design is more effective for the drag reduction. The optimized range of the length and angle of the base flap design is confirmed by a set of systematic CFD simulations and used as reference for future study to define the optimization design of this add-on device.

The objectives of this study are twofold. The first is to conduct the numerical experiments by using the baseline truck geometry to investigate the air flow characteristics, influences of mesh and flow mathematical models, and to find better configurations to reduce the C_d. The results from using the baseline will be used as a benchmark for later comparison with the simulations by attaching different types of the add-on devices. The second objective is to search for a set of optimal geometrical parameters of the base flaps to maximize the drag reduction.

In order to validate the effectiveness of the CFD simulations, the wind tunnel experiments with a 1:20 model of the truck were conducted at the University of Science and Technology of China (USTC) by a team of collaborators. The wind tunnel experiments produced similar results as the CFD simulations, which could be considered as a validation to the results from our CFD simulations.

Keywords: Class 8 truck, aerodynamic drag reduction, add-on device, CFD simulation

DEDICATION

This thesis is dedicated to all my family members and my sincere friends.

ACKNOWLEDGMENTS

First, thanks go to my advisor, the committee chair, Dr. Alan Shih, for all of his time and advice about my graduate study. Second, I would like to express my appreciation for the time, suggestions, and guidance from my committee members, Drs. Jong-Eun Kim and Roy Koomullil. Further, gratitude goes to Dr. Jianhua Wang and her graduate student, Fan Yang, from the University of Science and Technology of China, who led and performed the wind tunnel experiment described in this thesis.

I would like to acknowledge NASA's partial support through Constellation University Institute Project (CUIP) under Contract no. NCC3989 that allows me to study the computational geometry and mesh generation issues to gain knowledge that is crucial in this study.

To Tian Gan and all my sincere friends whose names have not been mentioned here, your help and support are acknowledged as well.

Last and most importantly, I would like to thank my family for their continuous and unconditional love and support, without which I could not have succeeded.

TABLE OF CONTENTS

Page

TABLE OF CONTENTS (CONTINUED)

LIST OF TABLES

Table *Page*

LIST OF TABLES (CONTINUED)

LIST OF FIGURES

Figure *Page*

LIST OF FIGURES (CONTINUED)

LIST OF FIGURES (CONTINUED)

LIST OF ABBREVIATIONS

CAD	Computer Aided Design
C_d	Drag Coefficient
CFD	Computational Fluid Dynamics
CO_2	Carbon Dioxide
DNS	Direct Numerical Simulation
DOE	Department of Energy
DOT	Department of Transportation
$k-\epsilon$	K – Epsilon
$k-\omega$	K – Omega
MPH	Miles Per Hour
RANS	Reynolds-Averaged Navier-Stokes
Re	Reynolds Number
RPS	Round Per Second
SST	Shear Stress Transport
U.S.	United States
USTC	University of Science and Technology of China

CHAPTER 1

INTRODUCTION

During the past few decades, the trend of increasing fossil fuel consumption, as well as the rise in fuel prices, have led to growing concern about vehicle fuel economy [1]. There are two major factors that contribute to such an upward trend, namely, worldwide economic growth and population increase. Moreover, due to such strong demand for fossil fuels in power generation and transportation, the output of carbon dioxide (CO_2) has significantly increased to a level that leads scientists to believe that it is a major contributor to the global warming phenomena observed in recent studies [2].

On July 29, 2011, President Barack Obama delivered an important policy remark on fuel efficiency standards for 2017-2025 year model vehicles during an event at the Washington Convention Center in Washington, D.C that resulted in a landmark agreement with automakers to set aggressive new fuel-economy standards for vehicles in the next decade, aimed to increase fuel efficiency by up to 10 percent and reduce fuel consumption by up to 380 million barrels every year [3]. This will yield $49 billion in dividends to our society. The standards will also reduce emissions of harmful air pollutants, which can lead to asthma, heart attacks, and premature death [4].

Heavy commercial trucking vehicles are critical to the economy as they transport goods in massive quantity. However, they are aerodynamically inefficient compared to other ground vehicles due to their large frontal areas and bluff-body shapes [5, 6]. It is

estimated that a regular 80,000 pound articulated Class 8 truck traveling at a normal highway speed of 70 miles per hour (MPH) consumes about 9 gallons of fuel to overcome drag across a 100-mile highway strip, while an average car would consume 4 times less in a similar situation [7]. In the United States (U.S.), according to an investigation by the Department of Transportation (DOT), 17% of the fuel consumed by all types of ground vehicles is done so by heavy vehicles that makes up only 1.1% of all road vehicles [8]. Therefore, it is critical to improve the fuel efficiency of these trucking vehicles to reduce the consumption of fuel.

One way to achieve this goal is to reduce the aerodynamic drag on the truck with novel designs on the geometry. As shown in Figure 1, contributions to the drag on a heavy trucking vehicle are mainly due to the net force associated with direct flow exposure on large tractor/trailer fronts, cross flow effects inside tractor/trailer gaps, complex underbody flow structure, and base wakes [3, 7]. According to the publication *Fuel Standards for Heavy Vehicles* [3], a common Class 8 truck moving at 70 mph expends 65% to 80% of its total energy overcoming the aerodynamic drag. Hence, even a small reduction in the aerodynamic drag could lead to substantial fuel saving. At the same time, the emissions of heavy trucks and concomitant fuel combustion can be significantly reduced. All in all, an improvement of a truck's configuration could decrease the drag coefficient (C_d), leading to a better fuel efficiency and a cleaner environment [2]. However, due to economic concerns, it is economically unfeasible to replace current fleets of Class 8 trucks with those with a re-designed, more streamlined body. The trailers are often standardized cargo containers, which also limit the changes

that can be made in a new design. Therefore, this study will focus on the resulting drag reduction on existing Class 8 trucks by the application of practical add-on devices [9].

For this study, a generic Class 8 truck geometry and add-on devices (cap fairing, skirt, boat tail, and flap) were designed and modeled using computer-aided design (CAD) software. Star-CCM+ [10], a CFD simulation tool, was used to discretize the computational domain using polyhedral meshes and compute the flow field parameters for use in deriving the coefficient of drag. Thus far, a large number of CFD simulations have been performed to study the flow characteristics and to reduce the C_d of vehicles. However, from the technical perspective, the CFD simulation is an approximate method to calculate the complex turbulence flow. Hence, it is necessary to conduct the corresponding wind tunnel experiments to validate the results from CFD simulations. Through the collaboration with researchers at University of Science and Technology of China (USTC), such experiments were carried out, and data are used in this thesis to validate the CFD simulations.

This thesis is therefore arranged in the following fashion to describe the problem, approach, and results. Chapter 2 provides an overview on CFD technology and its use in related applications by others through a proper literature review. Chapter 3 outlines the design of the generic Class 8 truck and its add-on devices from the geometric perspective. Chapter 4 describes the mesh generation process and flow parameter setup. Grid independence study is also discussed in this chapter to identify the proper grid size for use in the CFD simulations. Presented in Chapter 5 are the CFD results of various configurations and their comparison with wind tunnel results. Chapter 6 will provide a summary and conclusion of this study.

CHAPTER 2

LITERATURE REVIEW

2.1 Computational Fluid Dynamics

CFD is a well-established engineering discipline in the aerodynamic study of vehicles. Its main benefits, compared to wind tunnel experiments, are lower costs, faster turnaround time, and the fact that it can provide more detailed flow field data, or even animations of the complex flow fields. Hence, over the past three decades, substantial research focus and investments were injected into CFD technology development [11]. It is used widely today in flow field studies associated with both internal and external flows, with the flow speed ranging from subsonic to hypersonic conditions.

CFD tools can use many different types of meshes to discretize the computational domain. Commonly-used mesh types are block structured, tetrahedral, hybrid, hexahedral, and generalized meshes. Block structured meshes [42] were the mainstream mesh type in the 1980s and early 1990s due to their implicit connectivity and more efficient algorithm implementation in terms of memory usage, among other benefits. They are composed of structured hexahedral elements. However, due to the tedious mesh generation process associated with the use of this type of mesh in complex configurations, they are not used in daily industrial environment. The latest commercial CFD tools still support such mesh types, but users rarely use this type of mesh due to the laborious mesh generation process for complex geometry.

Tetrahedral meshes [13] require the grid connectivity to be explicitly defined, and they are considered less efficient than block structured meshes in general, especially in the early days when computer resources were limited in terms of computing power and memory size. Therefore, computations using this type of mesh were considered too expensive compared to block structured meshes. Its mathematical models for capturing flow features in boundary layers are also not as accurate as those using block structured meshes. However, due to its ability to allow easier and faster meshing for very complex geometry, its use has increased significantly as computer hardware resources increased in the past two decades.

Hybrid meshes [14] take advantage of the anisotropic meshing ability of a structured mesh and the ease of the mesh generation process of an unstructured mesh by allowing hexahedral, prismatic, pyramid, and tetrahedral elements to be used in a mixture to fill the computational domain. It in particular emphasizes the use of anisotropic mesh elements in the boundary layer to better capture the flow features near the walls.

Generalized meshes [15] further expand the mesh element shape to a general polyhedron, which allows the computational domain to be discretized by elements with any number of faces. Such generalization allows more efficient flow calculations. However, due to such generalization in element type, not all CFD tools can support it. The latest mainstream commercial tools do allow such generalized mesh elements.

There are also unstructured hexahedral [16] and Cartesian meshing [17] approaches used within the CFD discipline. However, they are beyond the scope of this study and will not be discussed in this thesis.

2.2 Previous Research in this Area

Skaperdas and Kolovos [18] presented a numerical investigation on the aerodynamic drag analysis of a car using the software ANSA, illustrated the method of investigating aerodynamic drag of the particular geometry by CFD. Regert and Lajos [19] exhibited a numerical result of the addition of wheelhouses and rotating wheels to optimize a car body. Lombardi et al. [20] presented an optimization procedure of a car aerodynamic configuration using a CFD aerodynamic solver. Through CFD simulation and a wind tunnel experiment, Ha et al. [21] examined the drag reduction by attaching different dimensions of rear flap add-on devices to a pick-up truck, thus representing an idea to achieve the optimum design by a set of systematic simulations. However, for heavy vehicles, there is a large potential to reduce the aerodynamic drag through optimization figuration design. In heavy vehicle studies, Daniel et al. [9] developed a family of structured and unstructured flow solvers to evaluate the effect of drag reduction devices (front spoiler and three mud-flap designs) on a full scale Class 8 truck using CFD solvers. However, the optimal design of base flaps was not concluded in their research.

2.2.1 Drag Reduction through Attach Add-on Devices

The use of aerodynamic add-on devices is the simplest but most effective approach to reduce the C_d because the cost is relatively low and the current truck structures and designs do not need to be changed significantly. It has been proven by Munson [22] that the pressure difference will be enlarged due to a pressure drop in the wake area behind the separation point, where vortices are generated. Specifically, the energy in wake will be consumed in rotation, which cannot be transformed to potential energy immediately.

This phenomenon will lead to the pressure difference surrounding the truck and result in an increased C_d.

Therefore, various add-on devices designed to reduce aerodynamic drag have been tried over the past few decades, such as sealing the gap between tractor and trailer, covering exposed underbody structures, adding base flaps to reduce wake and flow separation, etc. Although these approaches are achievable through installing a roof cap, side skirts, tractor-trailer seal, and base-flaps, some of these solutions have not been fully adopted in the trucking industry due to their immature designs. For example, side skirts make the truck underside less accessible for maintenance; a full roof cap is a good solution for articulated trucks, but would increase the drag when trailers are detached [6]. Furthermore, it is very difficult to identify an optimal base flap design to address many uncertain factors, especially for the base flaps/boat tail configurations. As a result, most of the previous studies on the aerodynamics of heavy trucks and add-on devices were mainly focused on understanding the flow characteristics around the trailer, as shown in Figures 1 and 2.

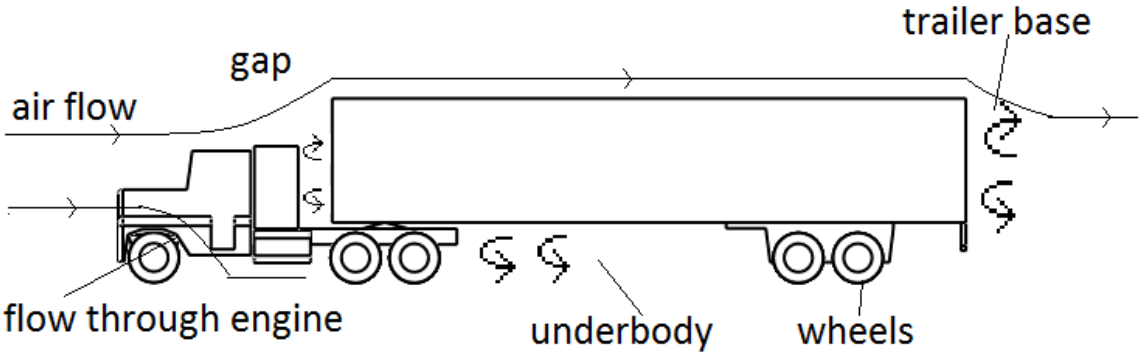

Figure 1. Several potential places to reduce the drag.

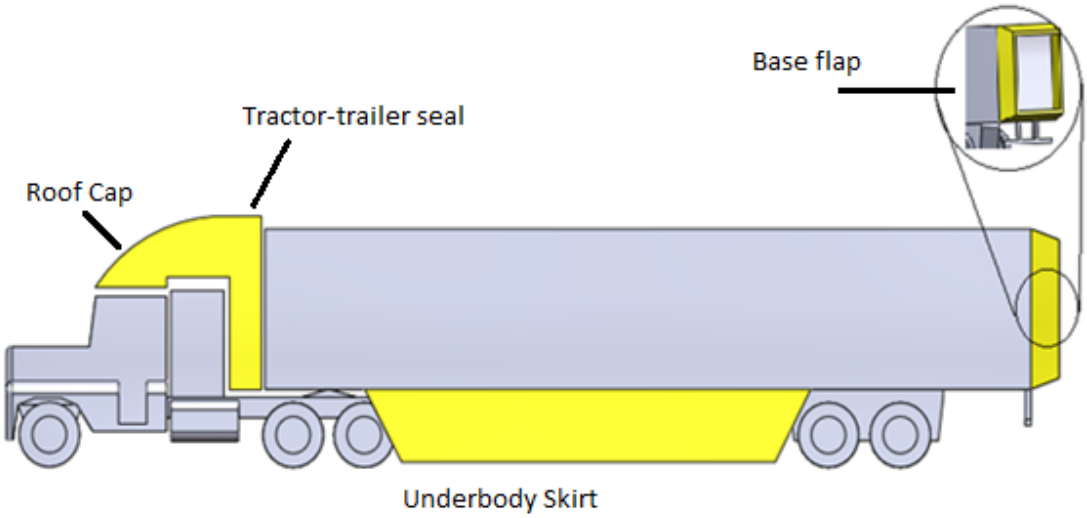

Figure 2. Examples of add-on devices used for reducing drag.

2.2.2 Physics Models Applied in CFD Simulation

It is widely acknowledged that turbulence models are inexact representations of the physical phenomena being modeled, and no single turbulence model is the best for every flow simulation [10]. Consequently, it is necessary to provide a suite of models that reflect the current state-of-the-art. In this study, the focus is on the investigation of the C_d of the truck, as well as the effect of the drag reduction of the add-on devices. Hence, we do not need to compute all of the detailed relevant physical scales in the simulations. Therefore, the RANS model was chosen as the turbulence model. On one hand, it is accurate enough to satisfy the need in obtaining the C_d values; on the other hand, the center processing unit (CPU) time will be much less compared with other turbulence models.

RANS is one of the most widely used equations in CFD simulations. To obtain the RANS equations, the Navier-Stokes equations for the instantaneous velocity and pressure fields are decomposed into a mean value and a fluctuating component. The averaging process may be thought of as time averaging for steady-state situations and ensemble averaging for repeatable transient situations. The main advantage of RANS is its relatively inexpensive computational cost; moreover, the numerical stability could be achieved with an appropriate models setting. Table 1 is a comparison of several widely used turbulence models, namely, the Direct Numerical Simulations (DNS) model, Large Eddy model, and RANS [12].

Table 1. Comparison between several widely used turbulence models.

Physics models	Advantages	Disadvantages
DNS	1. Compute all relevant physical scales	1. Very computationally expensive
Large Eddy	1. Simple subgrid models 2. Compute most of the relevant physical scales	1. Grid dependent 2. Relatively computationally expensive
RANS	1. Computationally inexpensive 2. Numerically stable 3. Grid independent	1. Overdamp unsteady flow 2. Complex model required

CHAPTER 3

GEOMETRY CONFIGURATION

There are many types of Class 8 truck designs, for which the C_d varies. In this thesis, one of the most typical models was chosen for investigation, as shown in Figure 3. The full scale geometric dimensions of the baseline model are shown in Figure 4. All of the parameters in the dimension are compliant with the limits set by the DOT. However, the detailed geometry in Figure 3 has some components on the truck that has less impact on the outcome of the C_d calculation. Therefore, after further modifications, a final geometry of the truck is shown in Figure 5.

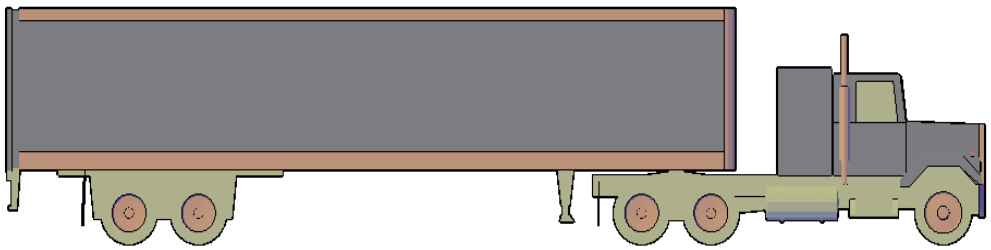

Figure 3. Original detailed geometry of the Class 8 truck.

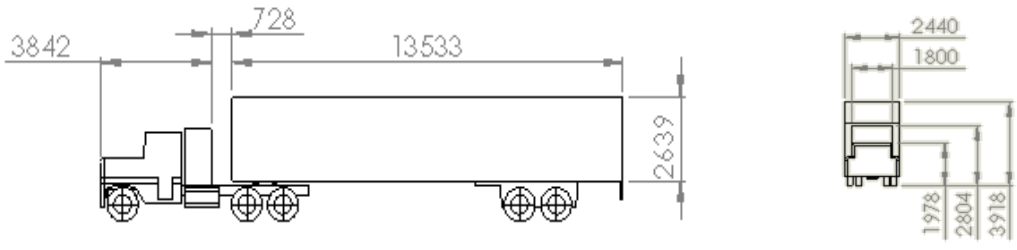

Figure 4. Key dimensions of the detailed Class 8 truck after modification (unit: mm).

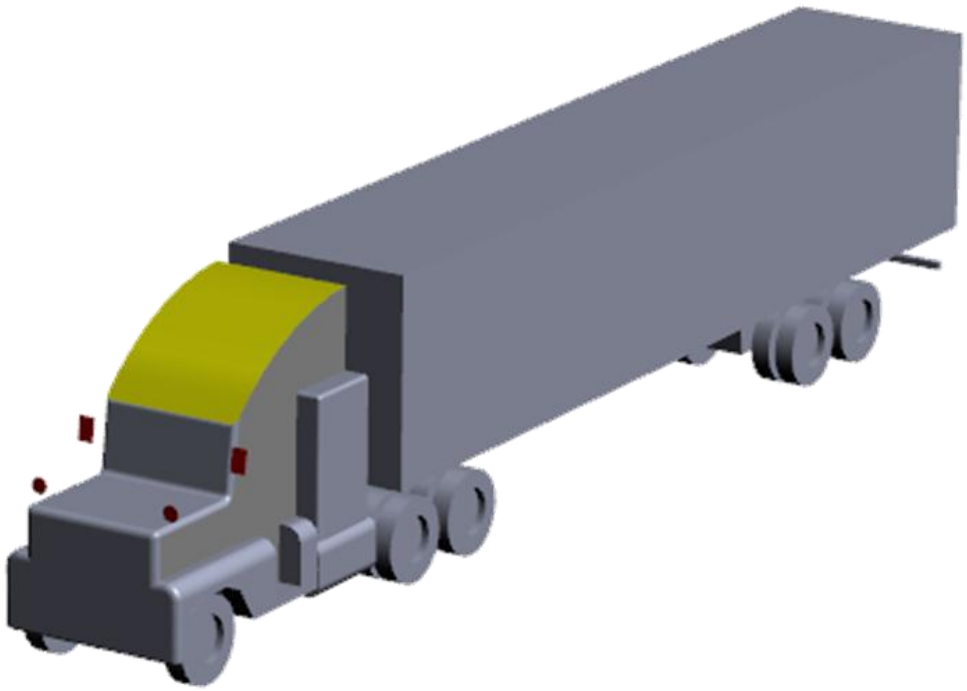

Figure 5. Final baseline geometry of the Class 8 truck.

From Figure 5 above, one can observe that several modifications were made to the original geometry in Figure 3, such as the lamp brackets, exhaust pipe, and fender board. The original detailed, complicated geometry could provide more precise results, but it would require a large CPU resource and the difference would not be significant. Therefore, an over-complicated geometry does not have to be used in this study as long as the geometry of significance in terms of flow characteristics are maintained. CPU time is dramatically reduced as well. In other words, by de-featuring unnecessary parts mentioned above, one can achieve a balance between the needs of simulation efficiency and accuracy.

3.1 The Add-on Devices

3.1.1 Boat Tail and Base Flaps

The geometries of the base flap and boat tail are shown in Figure 6. These two add-on devices were investigated often in the last decade [5]. The difference between the two add-on devices is that the base flap is opened in the rear of the trailer, while the boat tail is closed. Generally, the main variations in these two types of add-on devices are on its downward angle and length, as exhibited in Figure 7.

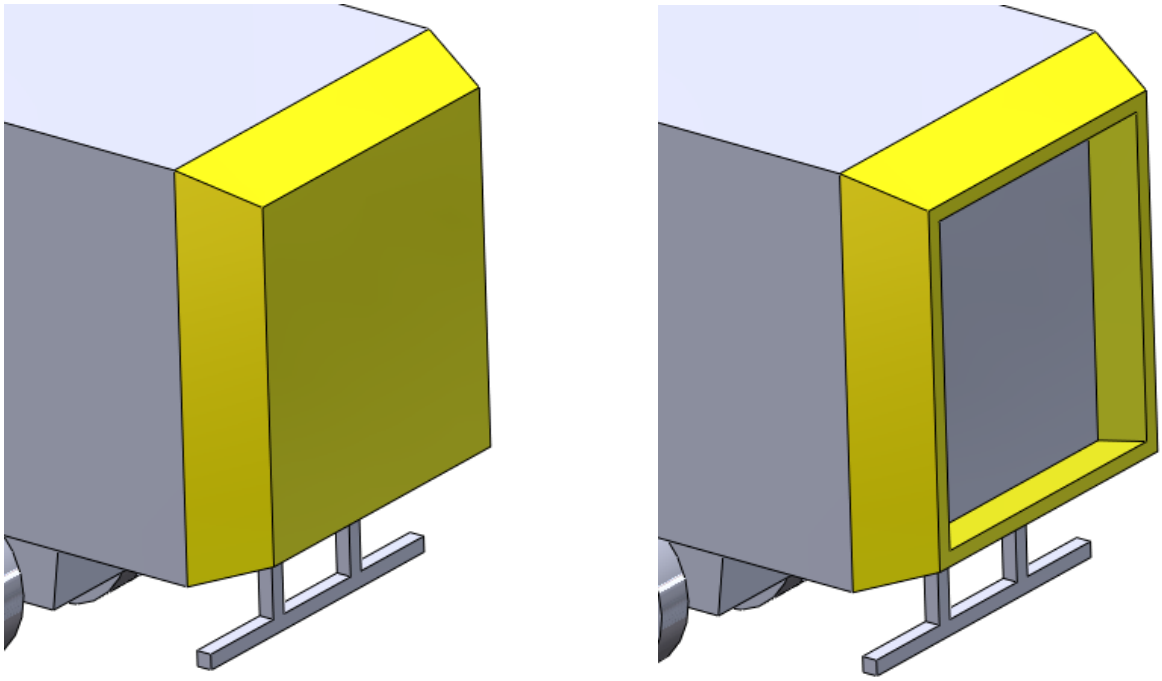

Figure 6. Geometry of boat tail (left) and base flap (right) devices.

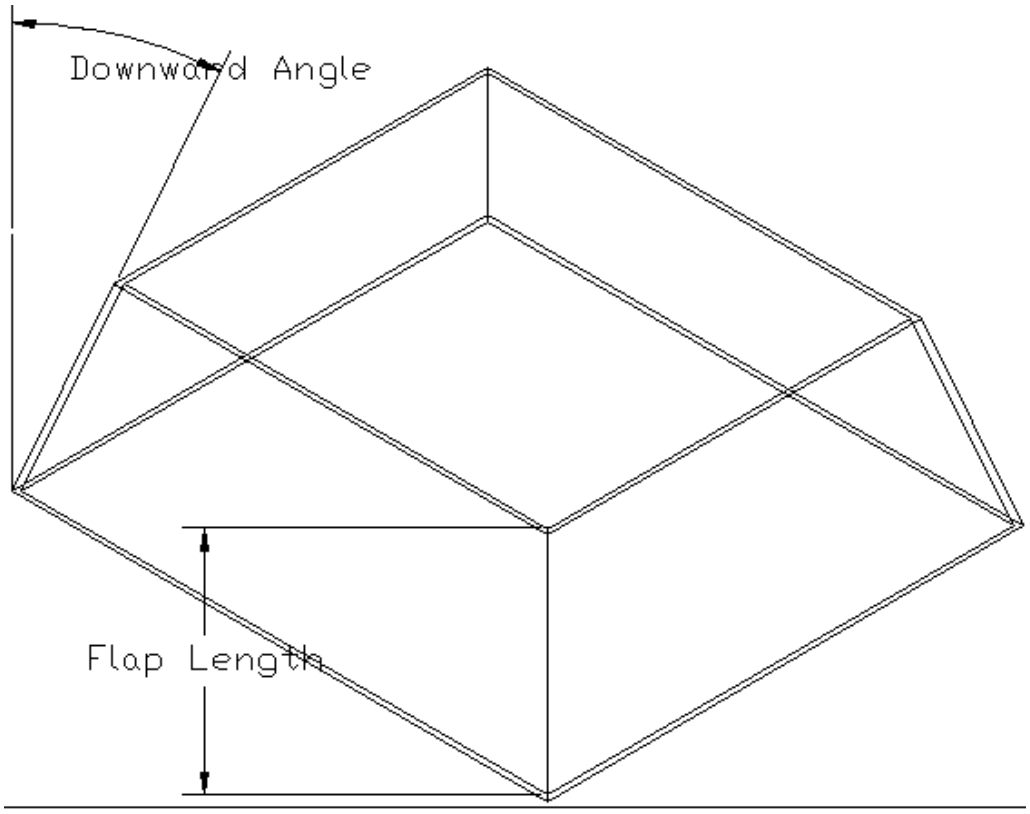

Figure 7. Design of the boat tail and base flaps.

According to an investigation by the Department of Energy (DOE), by using different angles and lengths for the tail/flap, one can obtain different results of the drag reduction [5]. However, it is very challenging to achieve the optimum design of the boat tail/base flaps from many uncertain factors. Taking the length of flaps for example, the vortices generated in the wake area behind the truck could be reduced if one uses a long flap, which leads to a decrease of the C_d; however, the pressure difference, as well as the skin friction, will be increased at the same time, which in turn increase the C_d. Hence, when taking all of these effects together, it is difficult to say whether the C_d will be

reduced under a certain circumstance [20]. Thus, previous studies on this issue have been mainly focused on the flow characteristic around the truck.

A better design could be achieved by conducting dozens of CFD simulations and/or wind tunnel tests. However, the design so obtained still has to be verified by the real truck road test [21]. The particular design of the add-on device could be changed along with different designs of the trucks. For example, the optimal design of a set of base flaps for a 15-meter long truck may no longer be optimal when attached to an 18-meter long truck, since the change in total length will influence the Reynolds Number (Re), which is a sensitive dependent factor of the C_d. The research of the optimal design of the add-on device is still in its initial state. However, according to previous simulation studies, the optimal angle of the boat tail/base flap lies in the range of $12°$ to $20°$, which provides an important guideline in the design of this study.

3.1.2 Underbody Skirt

The underbody skirt is very common on many trucks today, since it proved to be an effective approach to reduce the C_d. The skirt is easy to install and maintain. The geometry of the underbody skirt, which was attached to the baseline truck, is shown in Figure 8.

3.1.3 Tractor-trailer Seal

Similar to the underbody skirt, the tractor-trailer seal has been applied to many trucks. By attaching this add-on device, the vortex in the gap between tractor and trailer is reduced, which causes the drop of the global C_d. Moreover, it will not influence the Re.

However, the C_d of the truck will be increased when the trailer is detached. The seal will be detached to reduce the C_d in that case. The geometry of the tractor-trailer seal is shown in Figure 9.

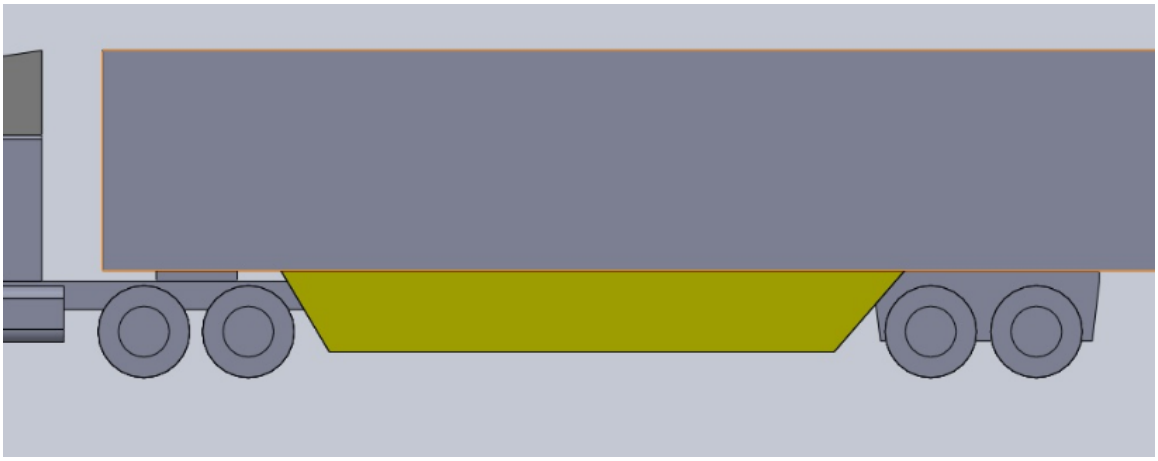

Figure 8. The underbody skirt.

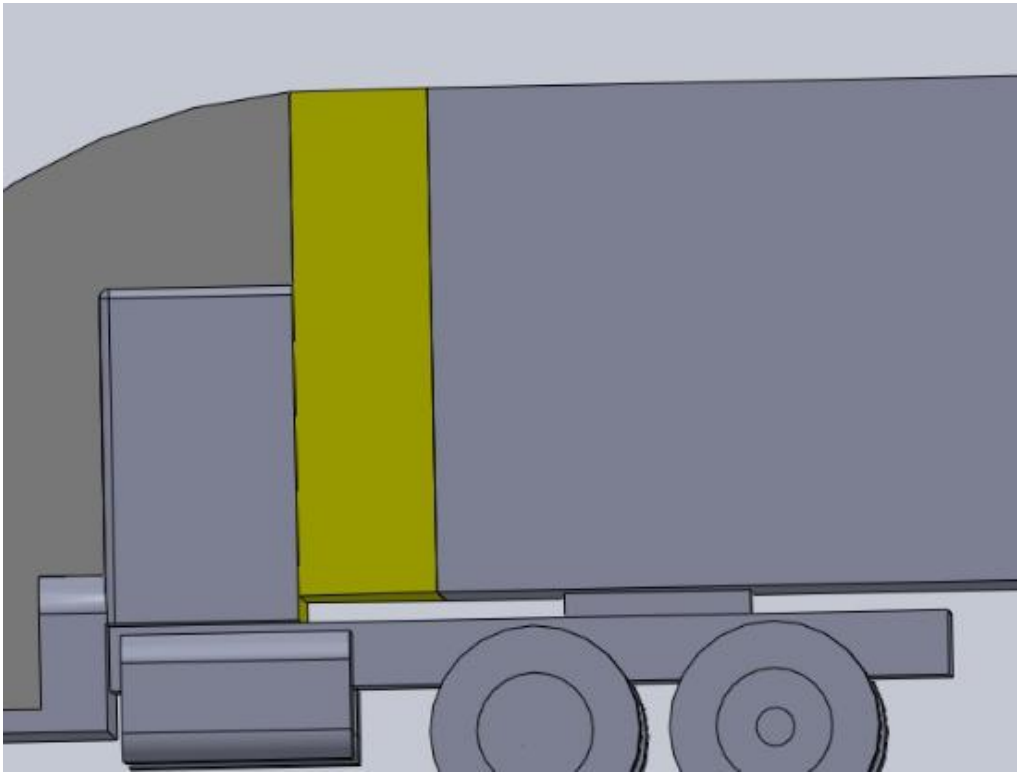

Figure 9. The geometry of the tractor-trailer seal.

3.1.4 Roof Cap

Drag reduction caused by the roof cap was proven during the last century. This type of add-on device could dramatically reduce the frontal pressure by trimming the flow, leading the drop of the pressure difference, and thus, decrease of the drag. Therefore, most Class 8 trucks have applied the roof cap. Hence, we applied this device in our study to make the overall calculation to be closer to realistic con Experimental study. The geometry of the roof cap for this study is shown in Figure 10. Note that the mirrors of the truck were kept in the simulations in this study.

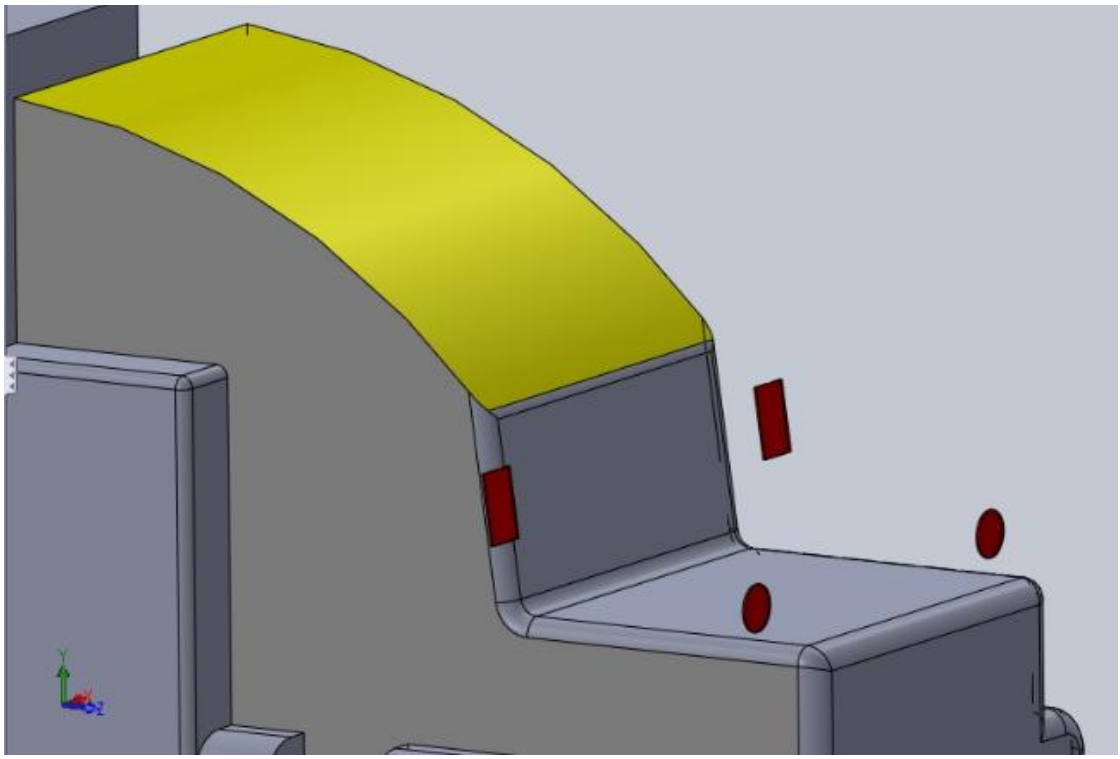

Figure 10. The geometry of the roof cap.

3.2 The Simplified Geometry

In order to establish the workflow and understand the simulation process in the beginning of this study, a simplified truck geometry was created to facilitate the process. It was used to understand the geometry design and formats, mesh generation requirements, grid dependent study, and selection of proper CFD parameters. The computational precision using this simplified geometry is not as good as the detailed one as one can expect. However, the principle of the numerical simulation is the same. Therefore, it helped to establish the simulation workflow. In other words, the simplified geometry also played a vital role in this study, which pointed the direction for the research associated with the detailed geometry. The simplified geometry is shown in Figure 11.

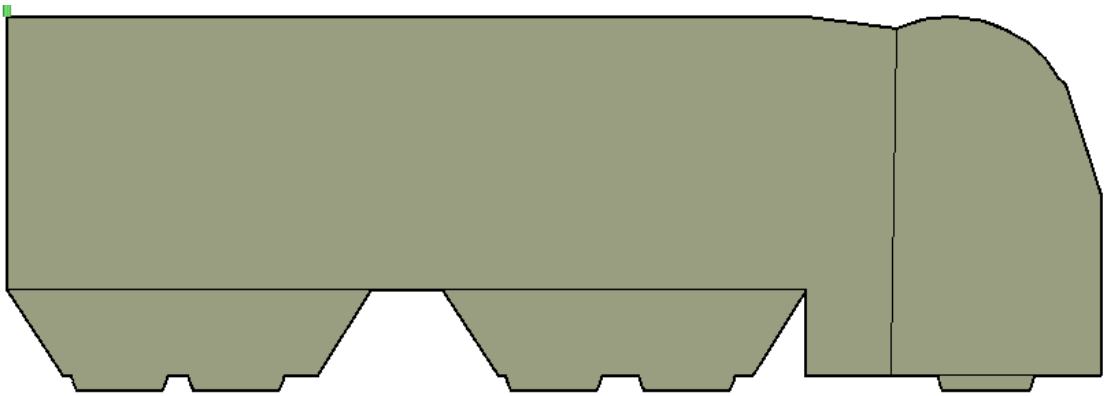

Figure 11. The simplified geometry used in the initial study.

CHAPTER 4

NUMERICAL APPROACH

4.1 CFD Software

The 3D flow field around the vehicle was numerically simulated using the commercial CFD software STAR-CCM+ v6.04. The simulations were based on the incompressible steady-state equations with the RANS model. In the beginning of this study, simulations were carried out by using the simplified geometry at a relatively low computational cost. Therefore, two turbulence models, both of the 2nd order realizable $k-\epsilon$ model and the 2nd order Shear Stress Transport (SST) $k-\omega$ model with segregated calculate flow were used in the simulations. From the comparison of the numerical results obtained by the two models, it was confirmed that the results from the SST $k-\omega$ model better exhibit the fluid flow behaviors at adverse pressure gradients and separating flow conditions. Moreover, the SST $k-\omega$ model can effectively reduce the possibility of solution divergence. The segregated calculation method was replaced with a coupled method, which takes more time, but provides better results. Therefore, in the detailed geometry simulations, the SST $k-\omega$ model was used, as shown in Table 2.

Table 2. Specific Physics Model used in this Study.

Physics model
Three dimensional
Turbulent
Incompressible
Steady state
Reynolds-Averaged Navier-Stokes
SST (Menter) K-Omega
Ideal Gas (Air)
Coupled Flow
Couple Energy
All y+ Wall Treatment
Gravity

4.2 Mesh Generation

The computational domain was established to be 10 characteristic lengths (10L) upstream, 20L downstream, and 10 characteristic widths (10W) to the sides, and approximately 15 characteristic heights (15H) in height, as shown in Figure 12, so that the entire domain could satisfy the free stream condition with zero normal gradients of all flow variables at the side and top faces.

However, in the systematic parametric study, the fluid domain does not have to be this large. The interference from the wall could be reduced by setting the motion of the

wall as translation, by giving a same velocity as the inlet. The specific method will be discussed in Chapter 5.

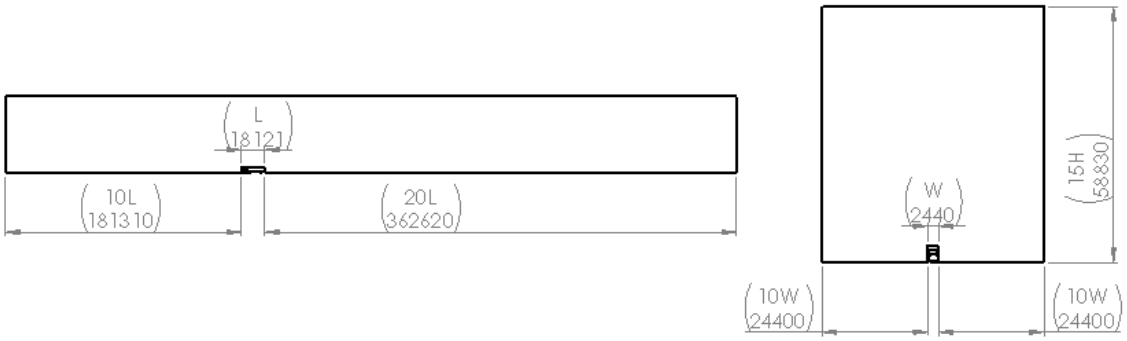

Figure 12. CFD fluid domain, side view (left) and front view (right); unit: mm.

The surface and volume meshes were generated using STAR-CCM+. The computational domain was discretized using polyhedral mesh elements, and prismatic boundary layers were extruded from the model surface into the computational domain. The aim was to reduce the numerical diffusion and to align with real flow near the model. The remainder of the domain was filled with polyhedral volume cells that were adjacent to the prism layers. To capture more details from the turbulence flow, some of the regions, where vortex happens, were refined. The specific mesh model included:

- Polyhedral Mesher
- Prism Layer Mesher
- Surface Remesher
- Surface Wrapper

4.2.1 Refined Mesh in the Critical Area around the Truck

Development of the high speed cluster computer, as well as the numerical simulation algorithm, allowed the simulation to be conducted with the mesh size up to 20 million. However, in order to obtain the essential information around the object in the fluid field, with the mesh size as small as possible to reduce the CPU time, the mesh was refined by concentrating most of the points around the truck, as shown in Figures 13 to 15. Table 3 shows the parameters of the fluid domain and the refined area.

Table 3. Main Parameters of the Mesh in Fluid Domain and Refined Area**.**

	Normal	Refined Area	Wheels
No. of Prism Layers	4	20	20
Base size	8.75m	0.1m	0.095m
Surface minimum size	0.875m	0.01m	0.0095m
Surface target size	2.8175m	0.04m	0.038m
Surface Curvature Rate	36	60	60
Thickness of the prism layers	0.6m	0.2m	0.2m

Prism layer stretching growth ratio = 1.20; m=meter

Notice that the wheels were treated as independent parts in the simulations. By doing that, one can obtain a better quality of the mesh around the wheels, especially at the points where wheels touch the ground, as shown in Figure 16. In the motion setting, the grid blocks of the wheels could be treated as rotational parts.

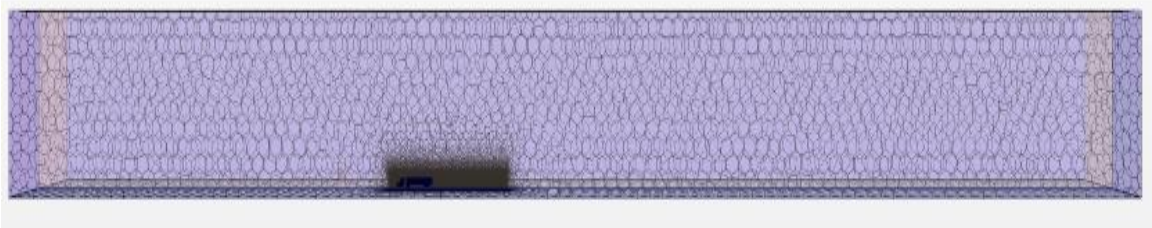

Figure 13. CFD mesh configurations, where the dark area represents the refined area.

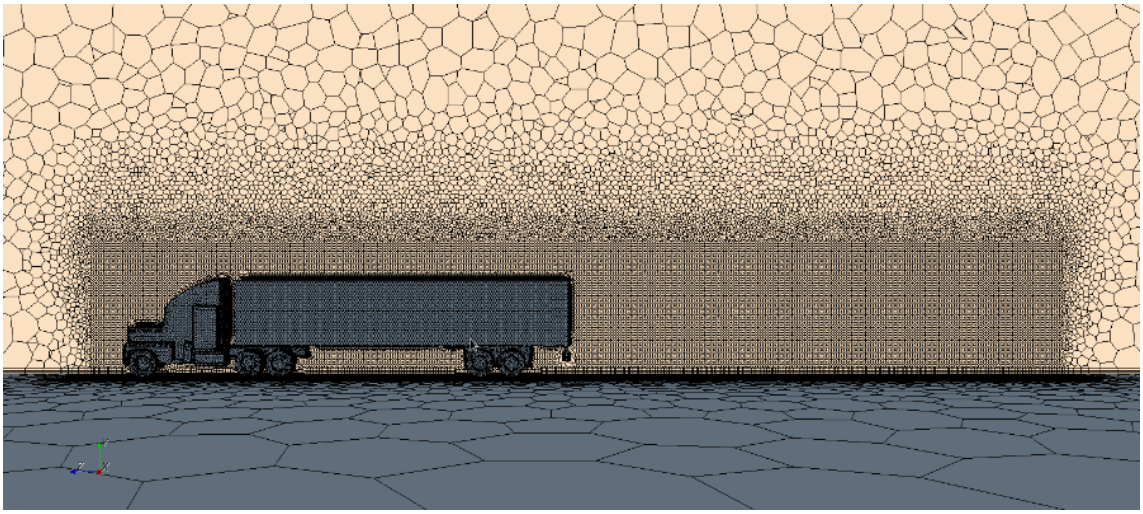

Figure 14. Refined mesh in the critical area around the truck.

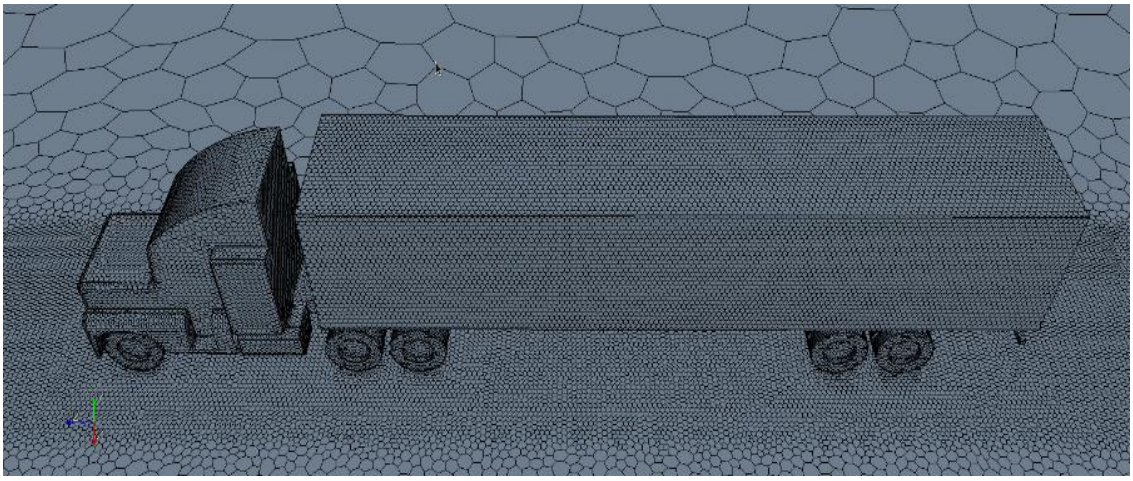

Figure 15. Refined mesh in the critical area, including the ground.

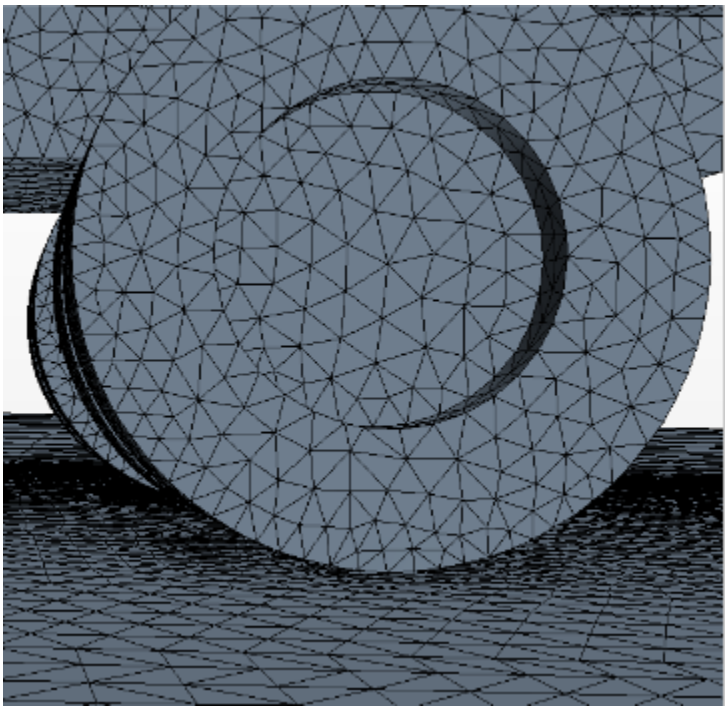

Figure 16. Mesh scene of the wheels.

4.2.2 Refined Mesh based on Solution

It is advantageous to refine the mesh based on some solution quantity (such as turbulent kinetic energy) in order to achieve successively more accurate solutions. The procedure for refining a mesh with solution is outlined in the following steps:

(1) Generate the mesh with refinements in critical areas.

(2) Run the simulation, and obtain the flow field result.

(3) Create a field function to return a mesh size value based upon appropriate solution.

(4) Refine the mesh based on the field function as weight for refinement.

(5) Repeat Steps (2) to (4) until the quality of the mesh is acceptable.

Figures 17 and 18 show the difference of the mesh with and without refinement based on the solution. These two figures use relatively coarse mesh, which allows one to distinguish the difference.

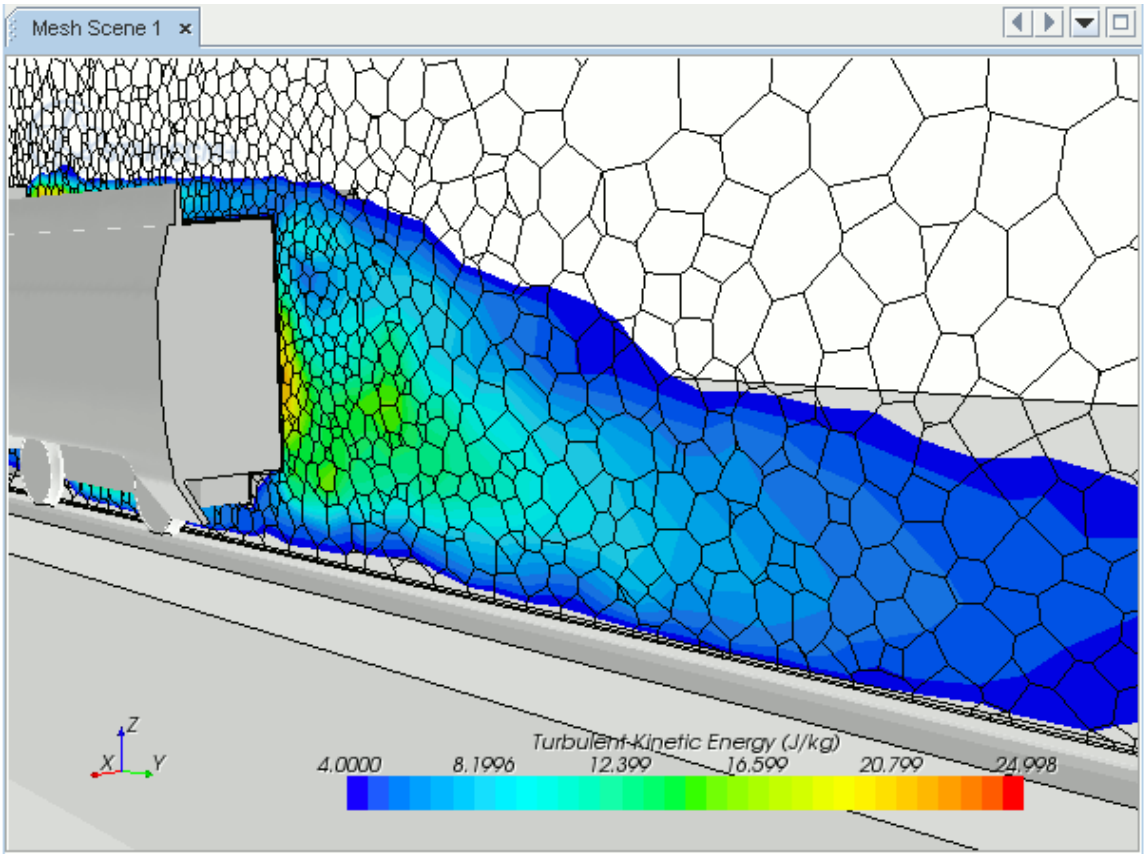

Figure 17. Mesh without the refinement based on solution.

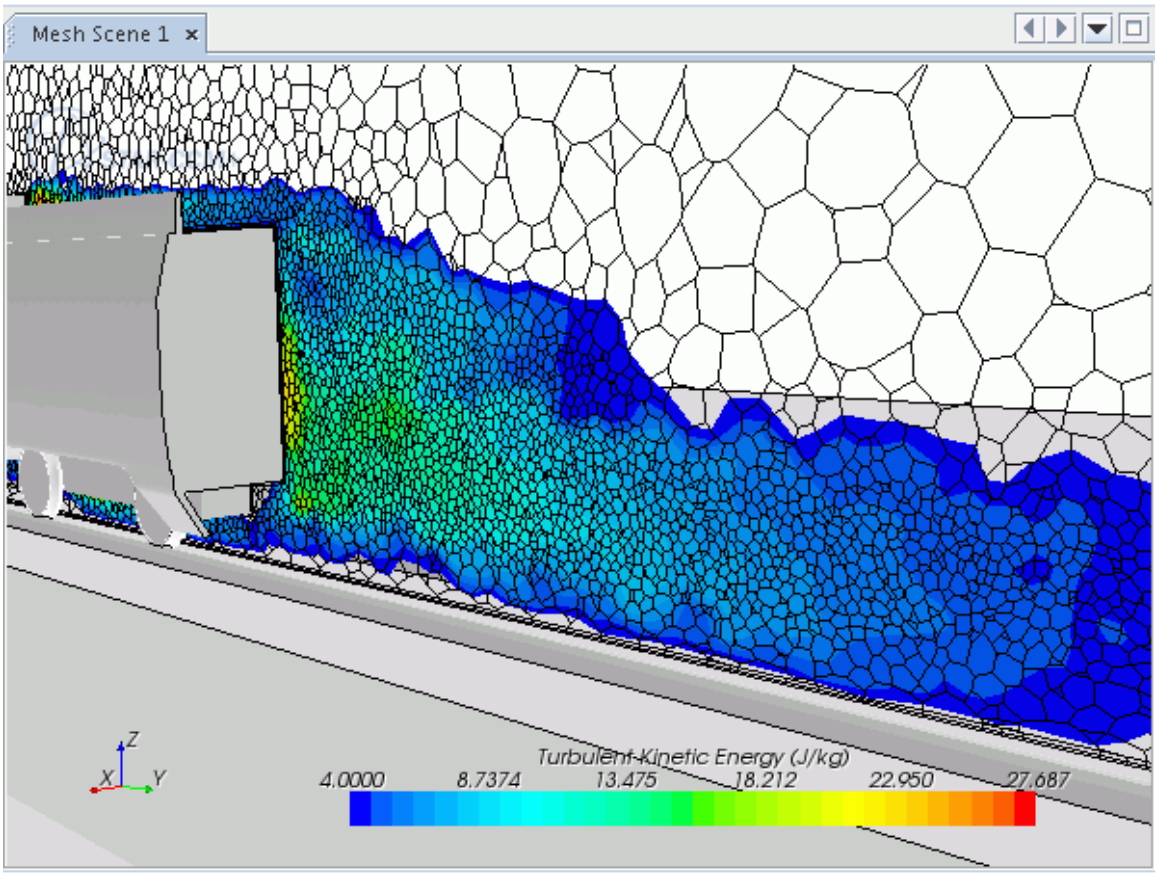

Figure 18. Mesh with the refinement based on the solution.

4.3 Grid Independence Study

The appropriate size of the mesh is one of the most important topics in CFD simulations. It is well known that the fidelity and details of the geometry, as well as the quality of the mesh, are essential in obtaining accurate solutions via the simulations [32]. Therefore, one must ensure that the details of the geometry are sufficient and the quality of the mesh is acceptable. Assuming the geometry details are sufficient, the simplest way to achieve accurate solutions is to increase the density of the mesh. However, if too many points are in the fluid domain, the CPU time will increase dramatically. For example, in

this study, generating a mesh with the size of 50 million polyhedral cells should be able to catch nearly all of the relevant scales of the turbulence. However, the simulation will take a long time to converge, which is not acceptable. Hence, the issue of identifying an appropriate size of the mesh that satisfies the needs for both the simulation accuracy and computational efficiency arises. The procedure for the grid independence study is outlined as:

(1) Import the geometry, and generate the mesh with necessary refinement.

(2) Run the simulation, and obtain the results.

(3) Increase the density of the mesh gradually, run the simulations, then obtain the results.

(4) Compare the results. If the difference between simulations is small enough, the mesh density is accepted.

The grid independence study for both the simplified and detailed geometry are shown in Figures 19 and 20, as well as listed in Tables 4 and 5.

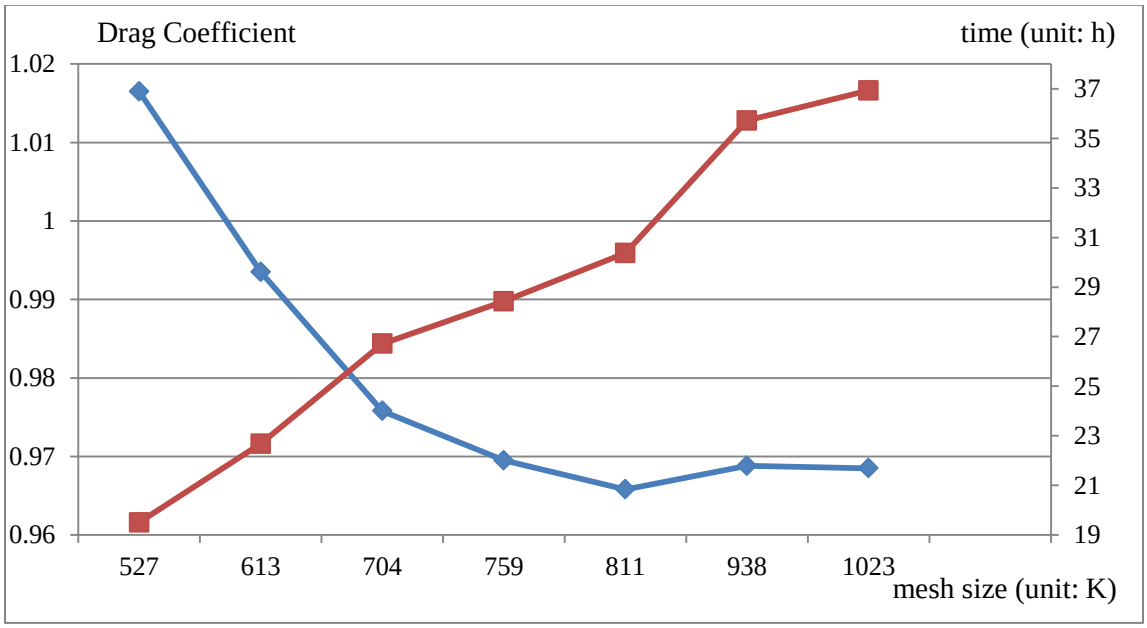

Figure 19. Grid independence test of the simulation with the simplified geometry.

The blue line in Figure 19 shows the resulting C_d, while the red line represents the computational time. It can be seen that the computation time increases almost linearly with the mesh size, while the variation in the C_d in two coarse cases is very large, but in the three fine cases, the differences of the numerical results are lower than 0.5%, which could be interpreted to be independent of the mesh sizes. The numerical results obtained with the larger mesh size would have higher resolution, but the costs in computing time increases dramatically. Therefore, the Fine-2 mesh strategy was chosen in the following simulations.

Table 4. Grid Independence Test, Simplified Geometry.

Case	Coarse1	Coarse2	Medium1	Medium2	Fine1	Fine2	Fine3
Size (K)	527	613	704	759	811	938	1023
C_d	1.0165	0.9935	0.9758	0.9695	0.9658	0.9688	0.9685
Time (h)	19.5	22.67	26.71	28.43	30.37	35.71	36.93
ΔC_d	N/A	0.023	0.0177	0.0063	0.0037	0.003	0.0003
ΔC_d in %	N/A	2.3150	1.8139	0.6498	0.3831	0.3097	0.0310

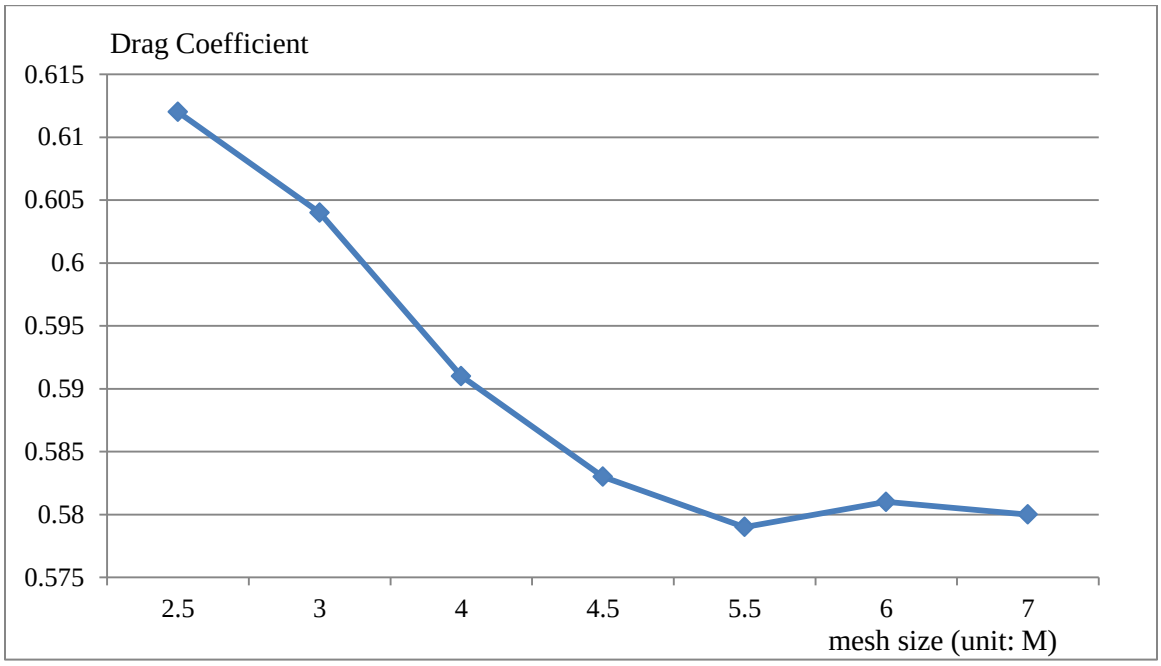

Figure 20. Grid independence test of the simulations with detailed geometry.

Table 5. Grid Independence Test, Detailed Geometry.

Case	Coarse1	Coarse2	Medium1	Medium2	Fine1	Fine2	Fine3
Size (M)	2.5	3.0	4.0	4.5	5.5	6.0	7.0
C_d	0.612	0.604	0.591	0.583	0.579	0.581	0.580
ΔC_d	N/A	0.008	0.013	0.008	0.004	0.002	0.001
ΔC_d in %	N/A	1.324	2.200	1.372	0.691	0.344	0.172

The principle of the grid independence study of the detailed geometry is exactly the same as the simplified geometry. However, most of the cases were carried out by a cluster computer, hence, the specific CPU time cannot be identified. Therefore, following the same procedure, the grid independence study was conducted for the detailed

geometry, as shown in Table 6. The Fine-1 mesh strategy was chosen to satisfy the needs for both accuracy and efficiency.

4.4 Physics Models Selection

As mentioned in Chapter 2, the RANS equation was applied as the turbulence model due to its inexpensive computational cost and numerical stability. However, the RANS requires a complex closure model, which has to be set properly. Several settings, such as the selection of the $k-\omega$ and $k-\epsilon$ models and wall treatment, had to be determined in this study.

4.4.1 Comparison Between the $k-\omega$ and $k-\epsilon$ Turbulence Models

The $k-\epsilon$ model provides a good compromise between robustness, computational cost, and accuracy. It is generally well suited for industrial-type applications that contain complex recirculation, with or without heat transfer. A $k-\epsilon$ turbulence model is a two-equation model in which transport equations are solved for the turbulent kinetic energy k and its dissipation rate ϵ. Various forms of the $k-\epsilon$ model have been in use for several decades, and it has become the most widely used model for industrial applications. Since the inception of the $k-\epsilon$ model, there have been countless attempts to improve it. One significant improvement is the realizable $k-\epsilon$ model, which was applied in the simulation with simplified geometry [10].

The $k-\omega$ model is similar to the $k-\epsilon$ model in that two transport equations are solved, but they differ in the choice of the second transported turbulence variable. The performance differences are likely to be a result of the subtle differences in these models,

rather than a higher degree of complexity in the physics being captured. The results of simulations by both of the $k-\omega$ and $k-\epsilon$ turbulence models with the simplified geometry are shown in Table 6 and Figure 21.

Table 6. Comparison of Results by using Different Turbulence Models.

Case	Coarse1	Coarse2	Medium1	Medium2	Fine1	Fine2	Fine3
Size (K)	527	613	704	759	811	938	1023
C_d $k-\omega$	1.0165	0.9935	0.9758	0.9695	0.9658	0.9688	0.9685
C_d $k-\epsilon$	1.0195	1.0023	0.9915	0.9846	0.9815	0.9837	0.9843

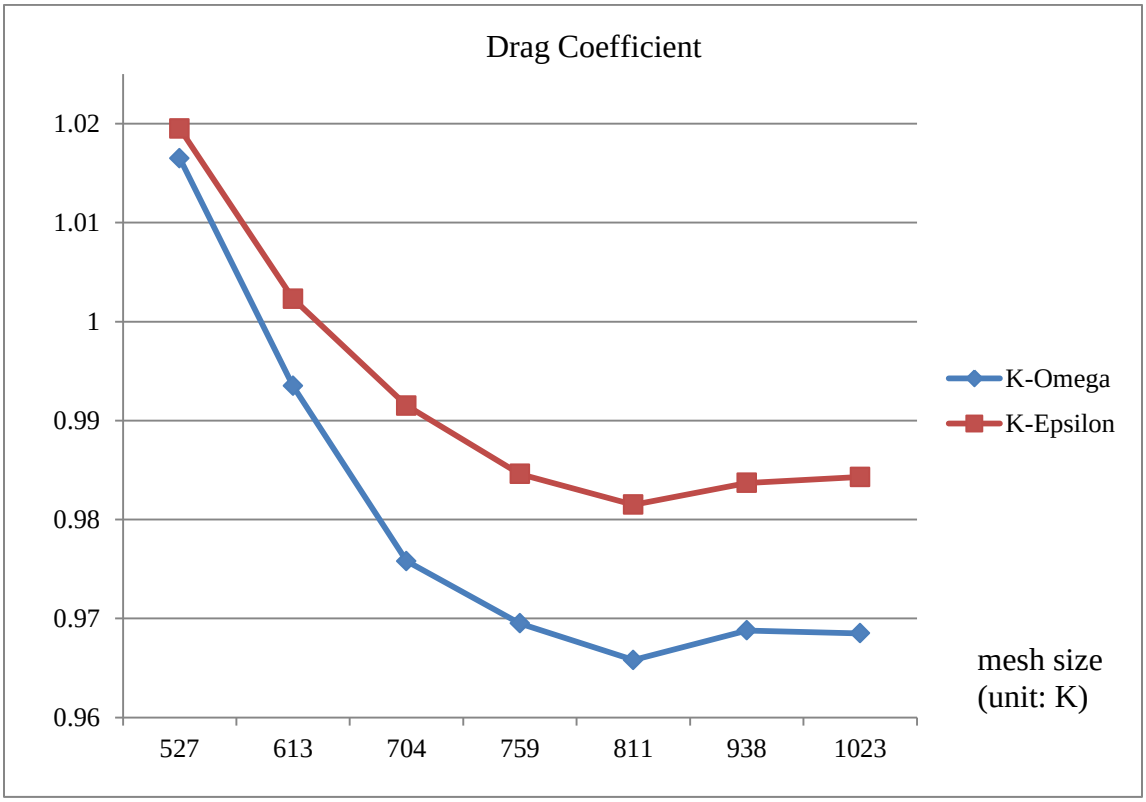

Figure 21. Comparison of C_d between the turbulence models.

As shown in Figure 21, the difference was not significant; both models could be applied to the detailed geometry simulations. However, the $k-\epsilon$ turbulence model caused divergence in the simulations for many cases, which might be due to the sensitivity to free-stream and inlet conditions. This was identified by Menter [38], who recognized that the ϵ transport equation from the standard $k-\epsilon$ could be transformed into an ω transport equation by variable substitution. The transformed equation is very similar to the one in the standard $k-\omega$, but it adds an additional non-conservative cross-diffusion term containing the dot product $\nabla k \cdot \nabla \omega$. Inclusion of this term ω in the transport equation will potentially cause the $k-\omega$ to give identical results to the $k-\epsilon$. Therefore, a blending function was introduced by Menter, which included the cross-diffusion term far from walls, but not near the wall. This approach effectively blends a $k-\epsilon$ in the far-field with a $k-\omega$ near the wall [36].

In addition, Menter also introduced a modification to the linear constitutive equation and dubbed the model containing this modification the SST $k-\omega$. The SST $k-\omega$ model has seen fairly wide application in the aerospace industry, where viscous flows are typically well resolved and turbulence models are generally applied throughout the boundary layer [10]. The SST $k-\omega$ model fits this study better than $k-\epsilon$, thus it was chosen as closure equations for further study.

4.4.2 Regions Setting

The fluid region for the detailed truck geometry was divided into several boundaries, including ground, inlet, outlet, truck, wall, and wheels, as shown in Figure 22. The physics settings of these boundaries are shown in Table 7.

Table 7. Physics Settings of the Boundaries in CFD Simulations.

	Physics model	Physics values
Ground	Wall	N/A
Inlet	Velocity Inlet	Velocity = 60MPH, Temperature = 293K
Outlet	Pressure Outlet	N/A
Truck	Wall	N/A
Wheels	Wall	Rotation Velocity = 7.632 Round per second
Wall	Symmetry Plane	Translation Velocity = 60 MPH

Moreover, the initial velocity of the fluid field was set as 60 MPH with a temperature of 293K, the same value as the velocity inlet. Note that the simulations associated with the simplified geometry were conducted using a range of velocities, namely, 50, 60 and 70 MPH. Through the comparison of these results from the study, C_d was confirmed to be independent of the velocity [12]. More detailed discussion is presented in Chapter 5.

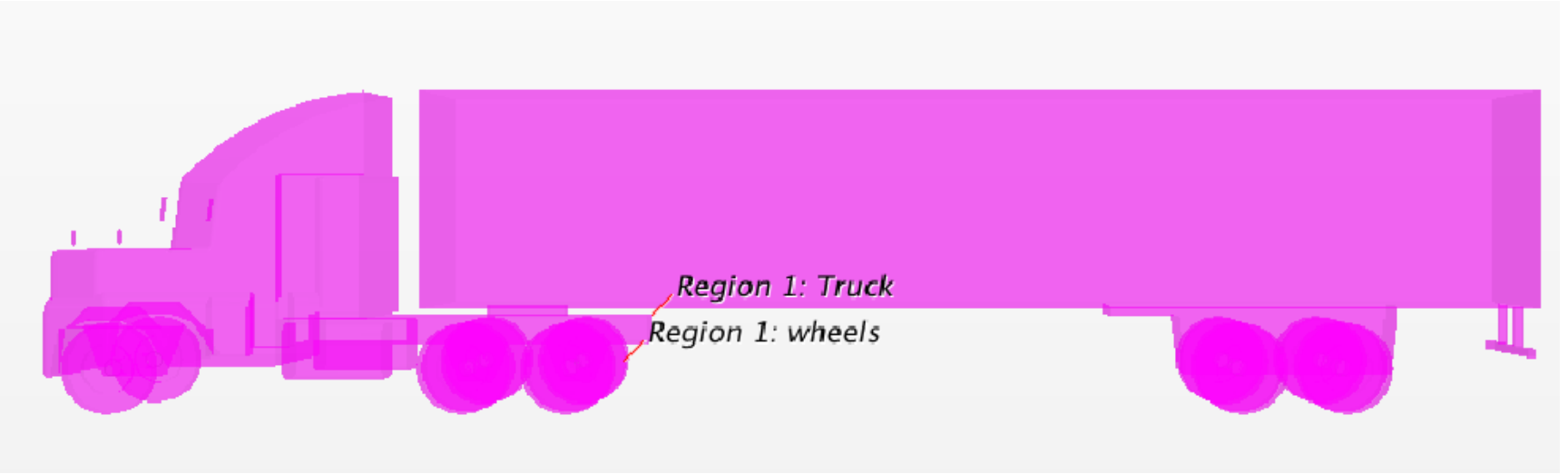

Figure 22. The separated boundaries in fluid regions.

4.5 Parametric Study

As previously mentioned, it is very challenging to obtain an ideal design of these add-on devices due to many uncertain factors, because the numerical simulation provides only one approximate solution. Hence, a parametric study simulation was conducted, aimed to identify an optimimal set of values to achieve the optimum design.

The parametric study begins with a geometry configuration generation with commercial CAD software. After this process, the variables to be optimized are inputted into the objective mode. Using the mesh software to generate a mesh, the simulation file is sent to the CFD solver and the aerodynamic drag is calculated at different conditions. The numerical results of the C_d are checked and analyzed manually. Based on the comparison of results from different cases, the trends of the variation of the C_d are identified. Then, following the trends, one optimal design should be defined. This procedure is continuously conducted until a satisfactory result is reached. In this study, the variables to be configured are the length and downward angle of the flaps. The objective is to obtain the minimum C_d for the entire geometry.

CHAPTER 5

RESULTS AND VALIDATIONS

5.1 Procedure to Obtain the Results

After the pre-processing steps were completed, which includes importing geometry, generating mesh, and setting up physics properties, simulations were conducted using STAR-CCM+. The number of iterations required for a particular case depends on several factors, such as the mesh size, the physics models, the under-relaxation factor, etc. For example, in the case where the mesh size is 4.5 million, as shown in Figure 23, the value of C_d oscillated significantly at the beginning of the simulation, especially for the first 1000 iterations, as shown in Figure 24. Therefore, the under-relaxation factor had to be set at a low value, as well as setting the flag ramp in the solver as linear to avoid divergence. When it comes to a relatively stable state, after 1500 iterations in this case, the under-relaxation factor could be set higher to speed up the convergence. When the C_d gradually reaches a stable value and the residual falls below the tolerance, the simulation is considered converged, and the computation would be concluded. Table 8 shows the specific values used for the under-relaxation factor and the ramp flag to conduct the simulations for all cases in this study. Figure 25 illustrates the oscillation behavior. Figure 26 is the graph of residual versus number of iterations. The nature of unsteady flow contributes to the fluctuation of the residual.

As one may observe, the value of C_d continuese to oscillate even when the simulation had converged with residule value smaller than the tolerance. However, the magnitude of such oscillation is small enough to be negligble. Therefore, in this demonstration case, the averaged value of the C_d from the last 1000 iterations is used as the final result. In this case, the value is 0.583.

Table 8. Specific Values Configured in the Solver for the Example Case.

	Beginning	Stable state	Final state
Under-relaxation factor	1.0	5.0	30.0
Ramp	Linear	Linear	N/A

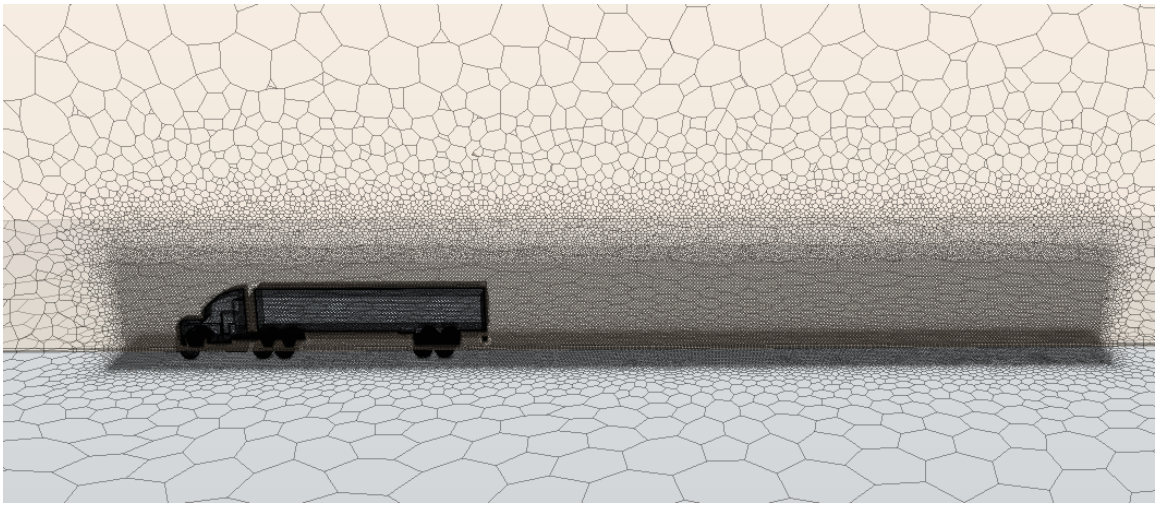

Figure 23. The geometry and mesh for the example case, mesh size = 4.5million.

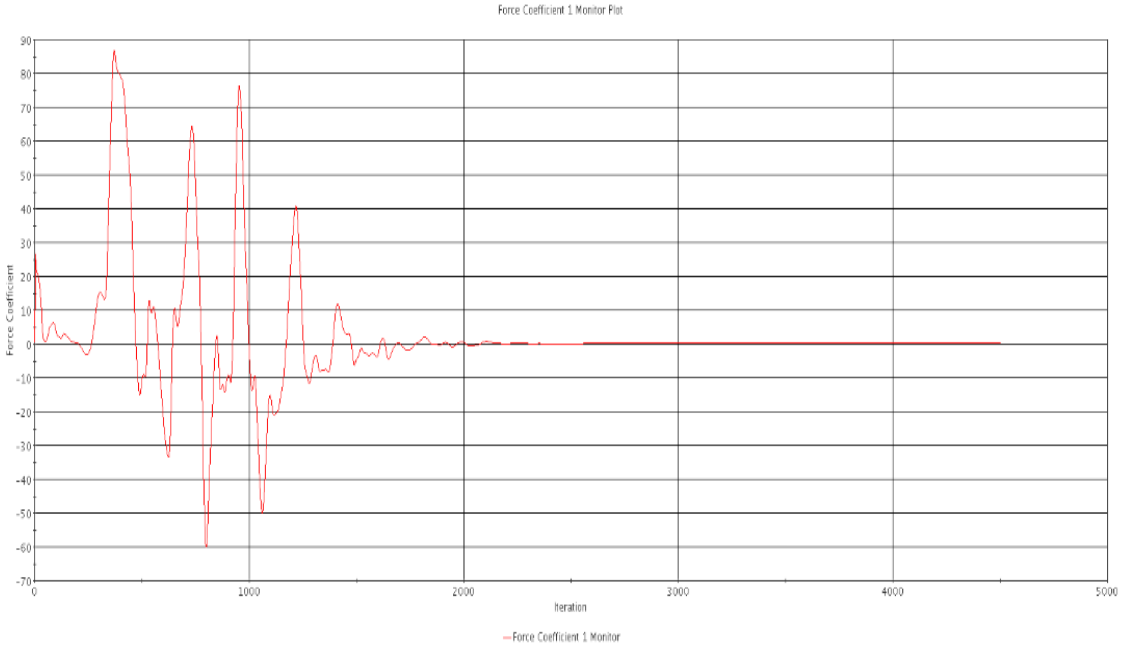

Figure 24. The plot of C_d versus number of iterations for the example case.

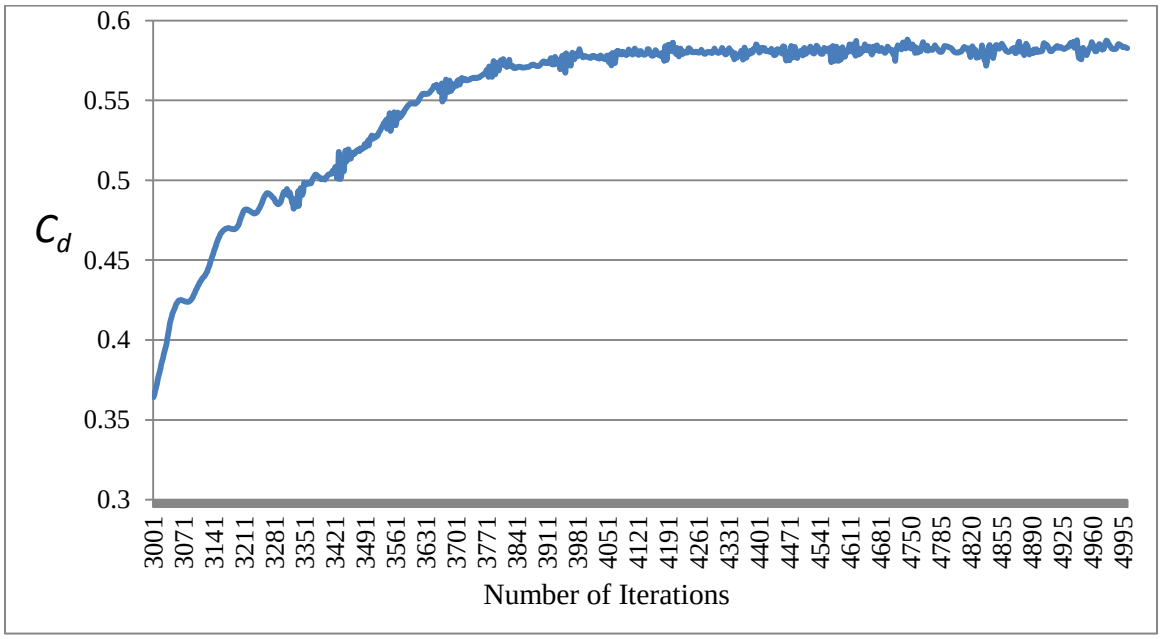

Figure 25. Plot of C_d versus number of iterations for the last 2000 iterations for the example case.

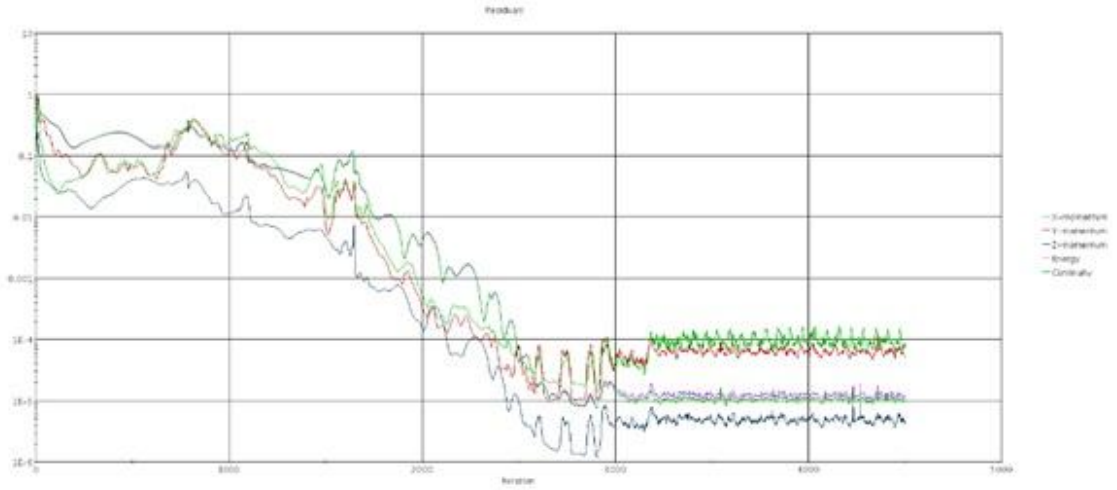

Figure 26. Plot of residual value versus number of iterations for the example case.

5.2 Simulations with the Simplified Geometry

Simplified geometry was used in this study mainly to explore the simulation process and understand the workflow in the beginning of this study. It helped to provide directions on how to improve the geometry of the add-on devices, how to set the CFD flow parameters, and what physics models to use in the simulation process, rather than to provide the details of the results. Hence, the numerical simulations were carried out at the beginning of this study with a set of base flaps and boat tails. The aim of which was to find the trends of the variation in the results. The lengths of the flaps and boat tail were normalized to the total length of the truck. Therefore, it does not matter if the total length of the truck varies from case to case. Table 9 shows the basic dimensions of the base flaps and the boat tail.

Table 9. Dimensions of the Base Flaps and Boat Tail Applied to the Simplified Geometry.

Length	0.015L	0.03L	0.045L	0.06L	0.075L	0.09L
Angle	8°	12°	16°	20°	24°	

The baseline simplified truck geometry, without add-on devices, had a C_d value of 0.9662. After setting the add-on devices, a new drag coefficient C_d' was obtained. To estimate the effect of the add-on devices, the relative reduction of the C_d is defined as:

$$\frac{\Delta C_d}{C_d} = \frac{|C_d - C_d'|}{C_d} \quad (1)$$

The relative reduction of the C_d was calculated at different lengths and angles for the base flap and boat tail configurations according to Eqn. (1), and the results are listed in Tables 10 and 11. Moreover, the comparison of the drag reduction between the base flaps and boat tail are shown in Figures 27 to 32 for different combinations of length and angle, aimed to quantify the variation of the drag reduction under different configurations.

Table 10. Reduction on C_d with Base Flaps (Simplified Geometry).

Angle \ Length	0.015L	0.03L	0.045L	0.06L	0.075L	0.09L
8°	5.408%	7.230%	8.834%	6.413%	8.140%	9.062%
12°	6.166%	8.100%	7.556%	5.757%	**9.777%**	8.104%
16°	7.376%	7.906%	8.441%	6.611%	5.216%	7.278%
20°	7.685%	5.295%	6.324%	5.640%	5.552%	5.795%
24°	5.996%	4.726%	3.972%	4.764%	4.310%	6.334%

Table 11. Reduction on C_d with Boat Tail (Simplified Geometry).

Angle \ Length	0.015L	0.03L	0.045L	0.06L	0.075L	0.09L
8°	6.531%	4.836%	4.411%	6.531%	8.041%	8.712%
12°	7.341%	6.073%	7.388%	7.338%	6.944%	8.003%
16°	4.810%	7.224%	7.105%	3.240%	4.204%	4.533%
20°	7.218%	4.792%	3.751%	2.054%	4.399%	6.251%
24°	6.233%	3.591%	3.169%	1.812%	3.814%	4.574%

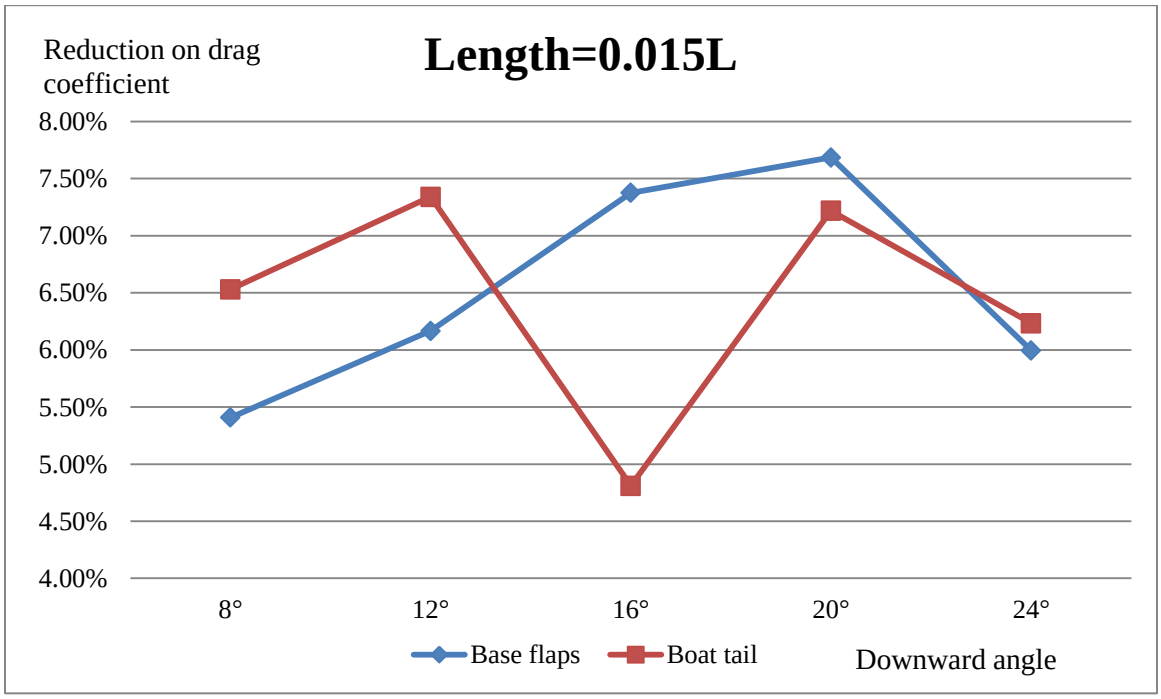

Figure 27. Comparison of the drag reduction, 0.015L, simplified geometry.

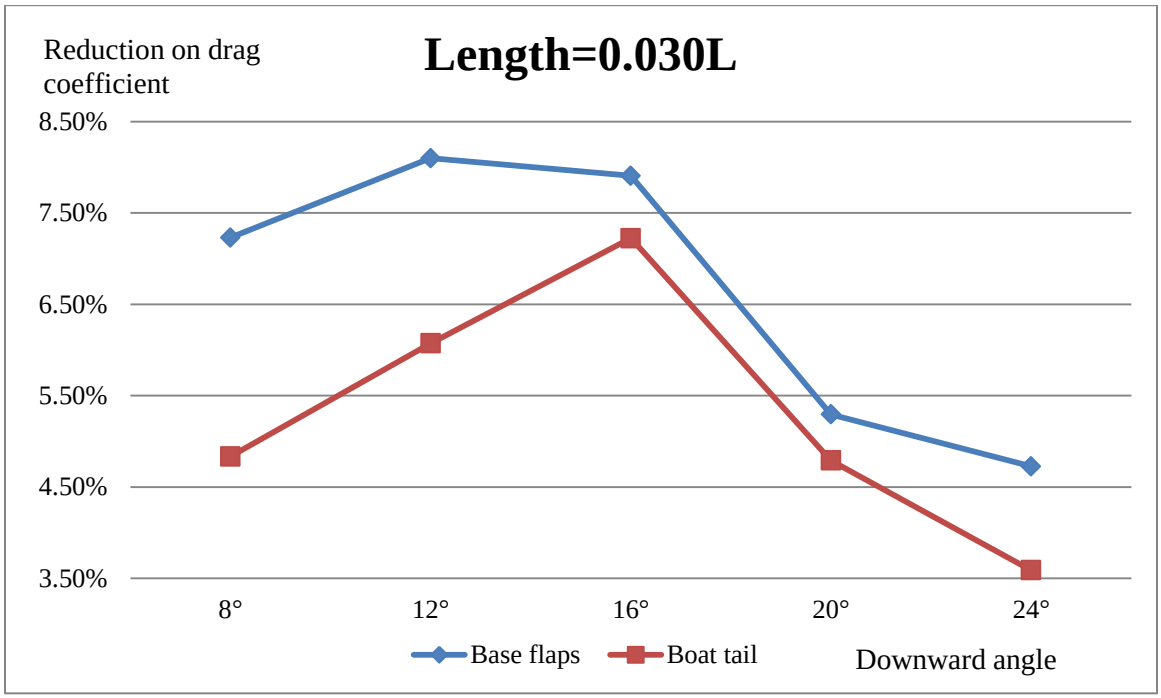

Figure 28. Comparison of the drag reduction, 0.030L, simplified geometry.

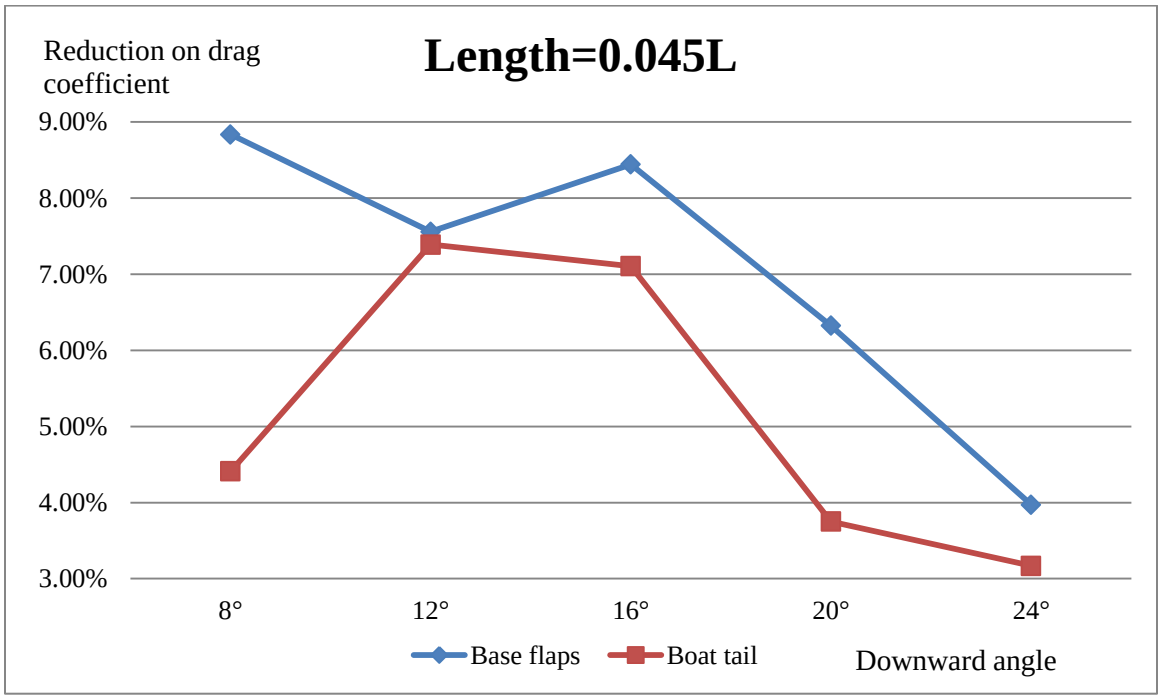

Figure 30. Comparison of the drag reduction, 0.045L, simplified geometry.

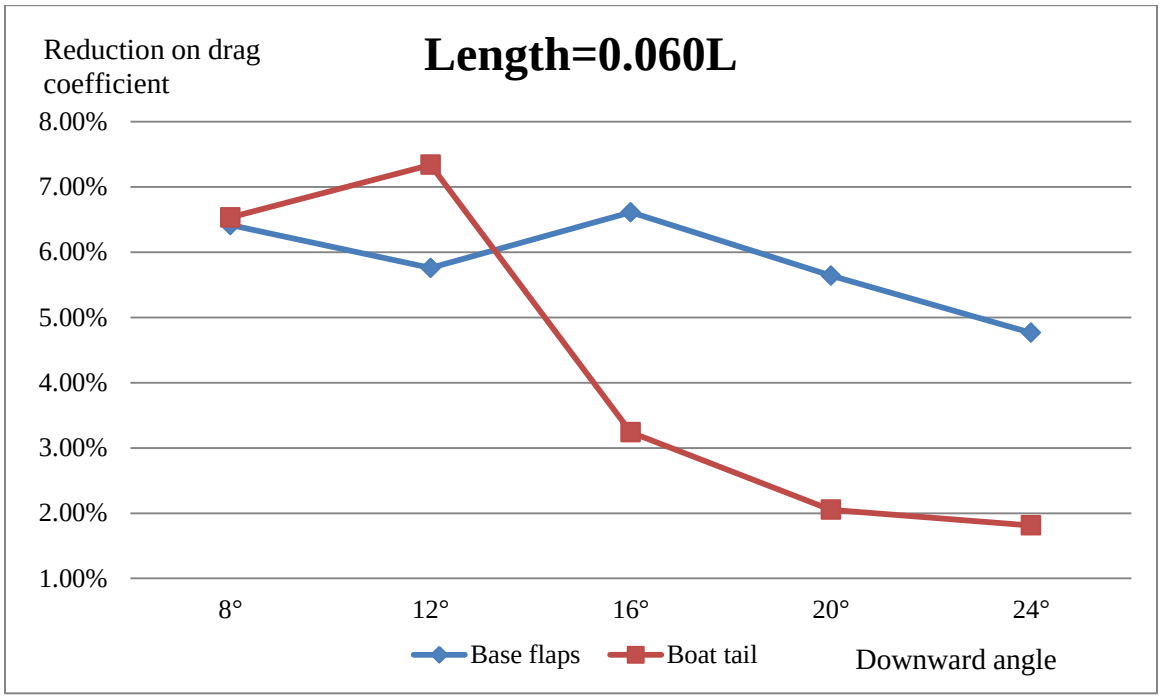

Figure 29. Comparison of the drag reduction, 0.060L, simplified geometry.

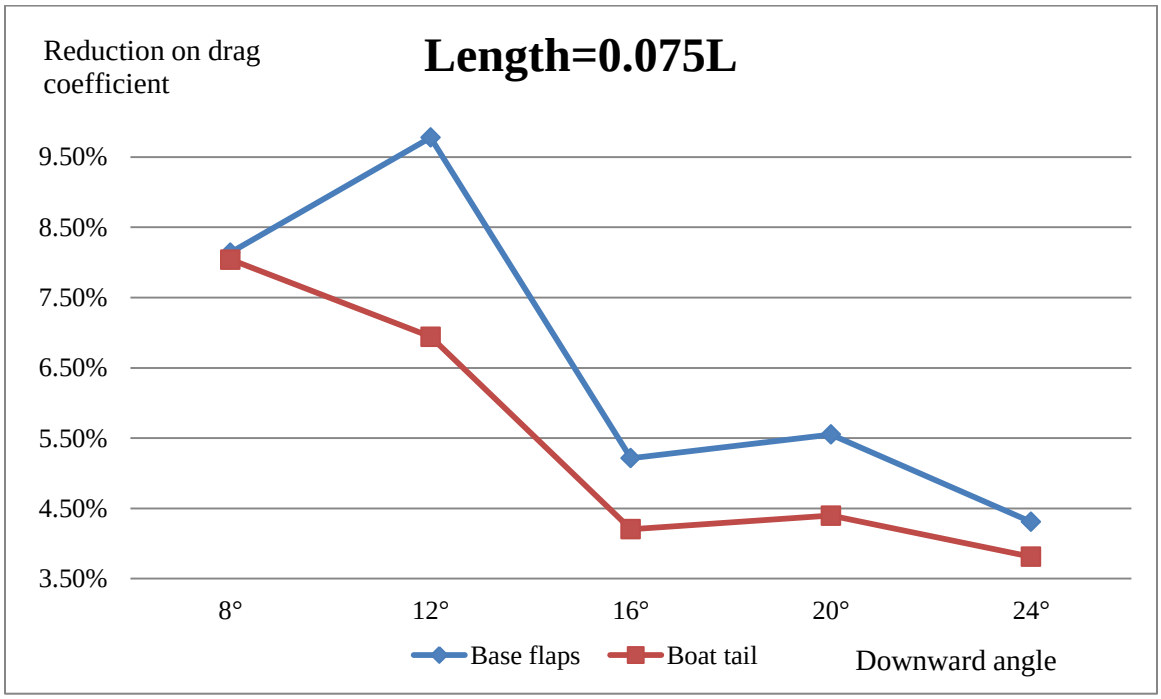

Figure 30. Comparison of the drag reduction, 0.075L, simplified geometry.

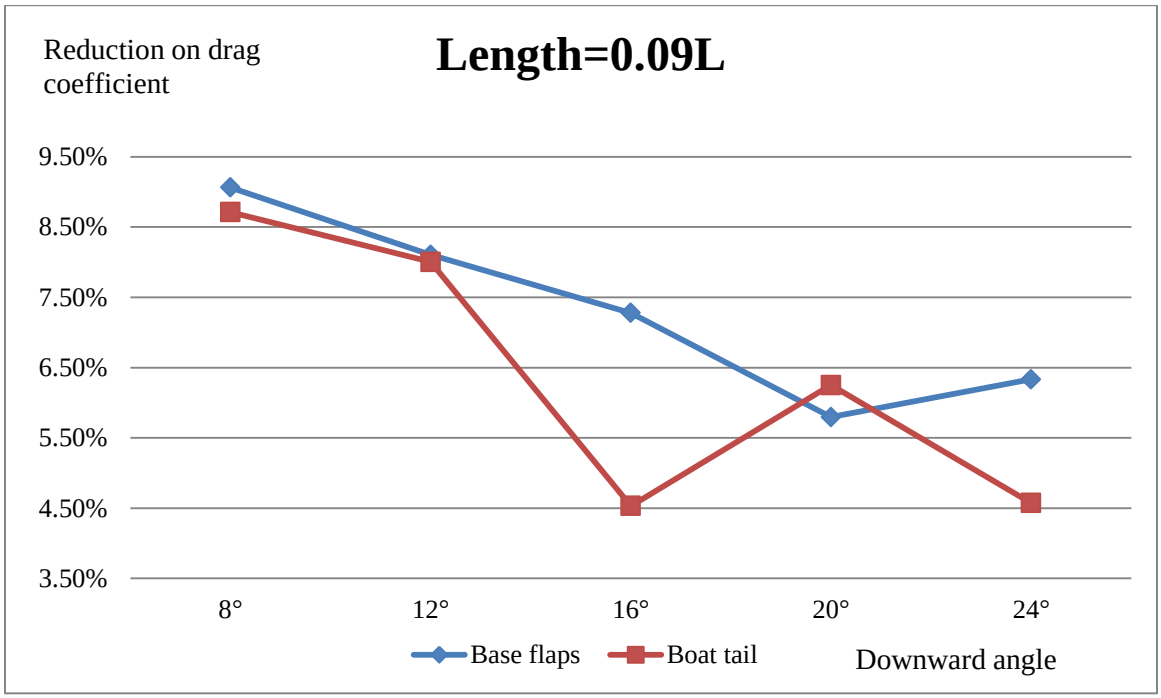

Figure 31. Comparison of the drag reduction, 0.09L, simplified geometry.

Through comparison of these results obtained by adding base flap or boat tail to the simplified geometry, two phenomena can be observed. First, although the boat tail has a slightly more complex geometry (closed geometry), the results suggested that the effect on the drag reduction seems to be less than that achieved by the base flap. The added cover plate does not improve the drag reduction. Therefore, in the following phase of this study, the focus was placed on the geometric design of the base flap configuration. The second phenomena observed that the maximum effect on the drag reduction (9.777%) exists in the region where the lengths were 0.06L and 0.09L and the angles were 12° and 20° as shown in Table 11. However, significant trends of the variation of the drag reduction could not been seen from the figures. This might be due to the relatively crude

geometry, the coarse mesh used, or the combination of both factors. That led to the parametric study with the detailed geometry with a focused range of 0.06L to 0.09L in length and 12° to 20° in angle.

5.3 Simulations with the Detailed Geometry

The initial simulations using the simplified geometry not only provided experience in conducting simulations associated with the truck geometry and its add-on devices, but it also helped to narrow down the range of geometric variations. This phase of the study started with the computation of C_d values of the baseline detailed truck geometry without any add-on devices. The C_d values were calculated with mesh sizes ranged from 4.0 million to 6.0 million (4.0M to 6.0M). After these values were obtained, each add-on device was added to the baseline detailed truck geometry to study its impact on the C_d reduction.

5.3.1 Underbody Skirt

The simulations with the underbody skirt were conducted in different mesh sizes, aimed to validate the grid independent study from another perspective. The mesh sizes varied from 4.3 million (4.3M) to 6.6 million (6.6M). The results are shown in Table 12, where the values of C_d of the baseline truck geometry (detailed) are compared with ones with the underbody skirt device. The relative drag reduction ratios are also listed in the table.

Table 12. Comparison between the Baseline and Configuration with Skirt.

Mesh size of baseline	C_d of baseline	Mesh size with skirt	C_d' with skirt	$\frac{\Delta C_d}{C_d}$
4.0 M	0.591	4.3 M	0.571	3.38%
4.5 M	0.583	4.9 M	0.551	5.49%
5.5 M	0.579	6.0 M	0.553	4.49%
6.0 M	0.581	6.6 M	0.544	6.37%

The increase of the mesh size from the baseline case is due to the addition of the underbody skirt itself, so that the overall mesh about the baseline truck geometry is not altered significantly. Otherwise, significant mesh size changes and arrangement of the meshes near the truck body could jeopardize the numerical results and make the outcome difficult to interpret and become less conclusive. Despite the fact that the first case at 4.0M mesh size suffered some mesh quality issues, due to the coarseness of the meshes, one can observe that the C_d value with the underbody skirt is around 0.55, with a reduction of C_d around 5.5%.

5.3.2 Tractor-Trailer Seal

Following the same procedure as the underbody skirt, a simulation was conducted for the configuration with the tractor-trailer seal, but with a mesh size of only 5.5 million. The result is shown in Table 13. The reduction on drag could achieve to around 9.50% with the tractor-trailer seal in this case.

Table 13. Comparison between Baseline and Configuration with Tractor-Trailer Seal.

Mesh size of baseline	C_d of baseline	Mesh size with seal	C_d' with seal	$\frac{\Delta C_d}{C_d}$
5.5 M	0.579	6.3 M	0.524	9.50%

5.3.3 Base Flaps and Boat Tail

According to the results from the simulations with simplified truck geometry, the base flap design has a better outcome on drag reduction than the boat tail design. Moreover, the potential optimal design of the base flaps on the drag reduction exists in the range of 0.06L and 0.09L in length and 12° and 20° in angle. Therefore, they are used as the range in a systematic study, aimed to achieve the maximum drag reduction. Furthermore, simulations were conducted with different configurations of the boat tail design, to examine its effect of drag reduction. At different length and angle combinations for the base flap and boat tail configurations, the relative reductions of the C_d were calculated, and the results are listed in Tables 14 and 15.

Table 14. Reduction on C_d with Base Flaps (Detailed Geometry).

Angle \ Length	0.06L	0.07L	0.08L	0.09L
12°	14.076%	16.079%	16.995%	18.618%
14°	10.777%	20.449%	22.314%	20.777%
16°	17.910%	21.762%	25.907%	24.283%
18°	20.587%	**28.497%**	24.870%	26.131%
20°	22.902%	22.349%	21.779%	22.781%

Mesh size of baseline = 5.5 M; Mesh size with base flaps/boat tail = 6.7M

Table 15. Reduction on C_d with Boat Tail (Detailed Geometry).

Angle \ Length	0.06L	0.07L	0.08L	0.09L
12°	15.405%	15.231%	19.563%	16.132%
14°	16.749%	14.285%	21.316%	16.604%
16°	18.602%	15.512%	**22.781%**	17.335%
18°	14.306%	19.424%	15.346%	16.173%
20°	20.341%	17.305%	21.435%	18.415%

The maximum drag reduction of the base flaps, 28.497%, was achieved at the combination of 0.07L and 18°. At the same time, the drag reduction of the boat tail design could only achieve as much as 22.781%. The plots of the reduction on C_d, at each length, are shown in Figures 32 to 35. From these figures, one can observe that the

reduction of the C_d improved as the angles increased, in general. The base flap design has a better outcome on the maximum drag reduction than that of the boat tail design. From Figures 33 to 36, it is obvious that the drag reduction of the base flaps design is better than the boat tail design, in general. This observation confirmed the same observation with simplified geometry.

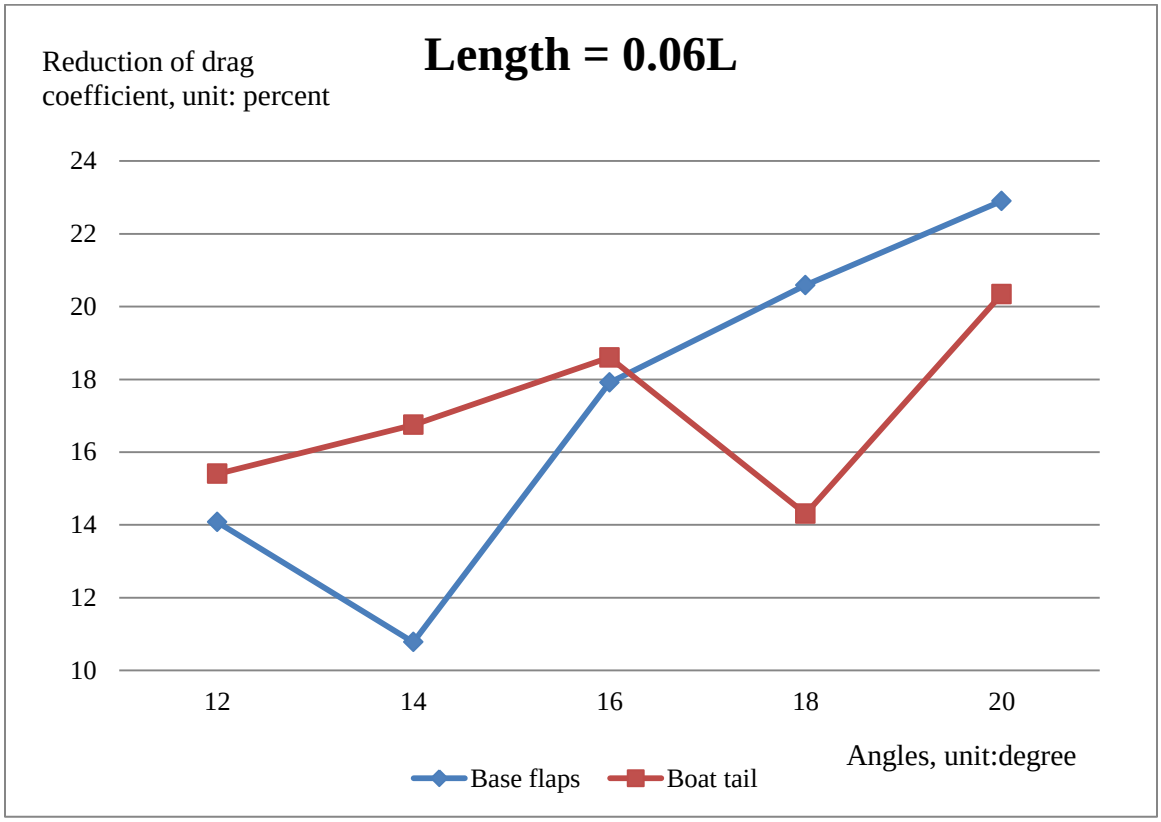

Figure 32. Comparison of the drag reduction, 0.06L, detailed geometry.

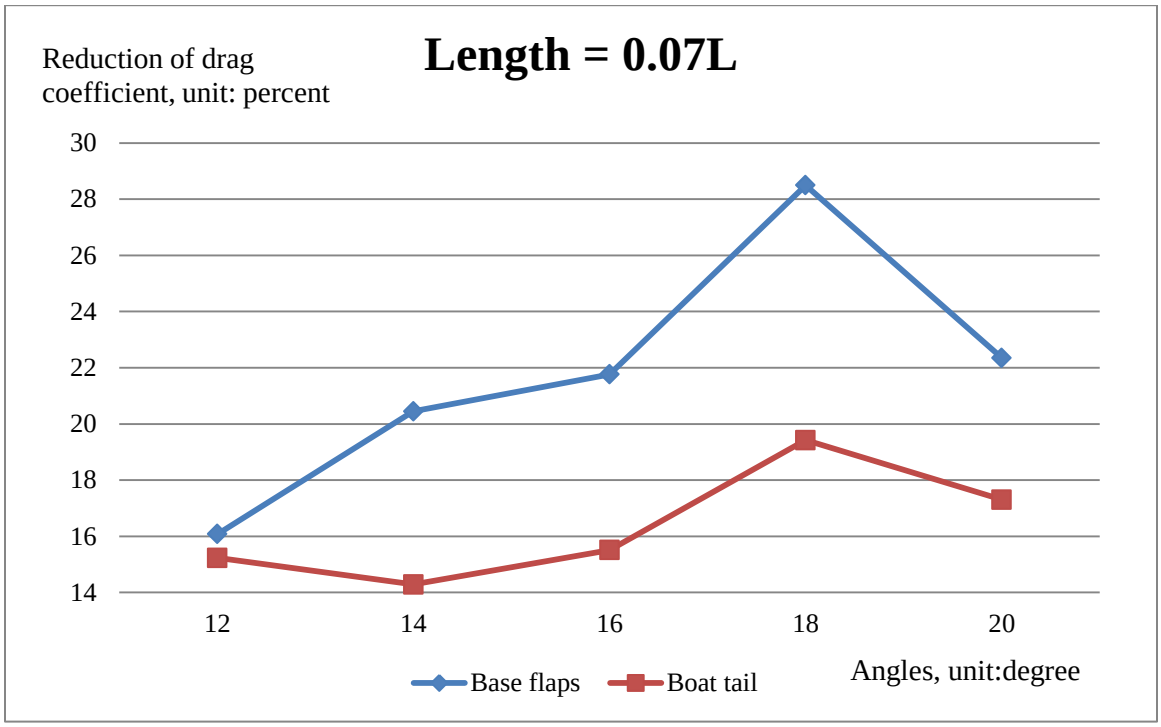

Figure 33. Comparison of the drag reduction, 0.07L, detailed geometry.

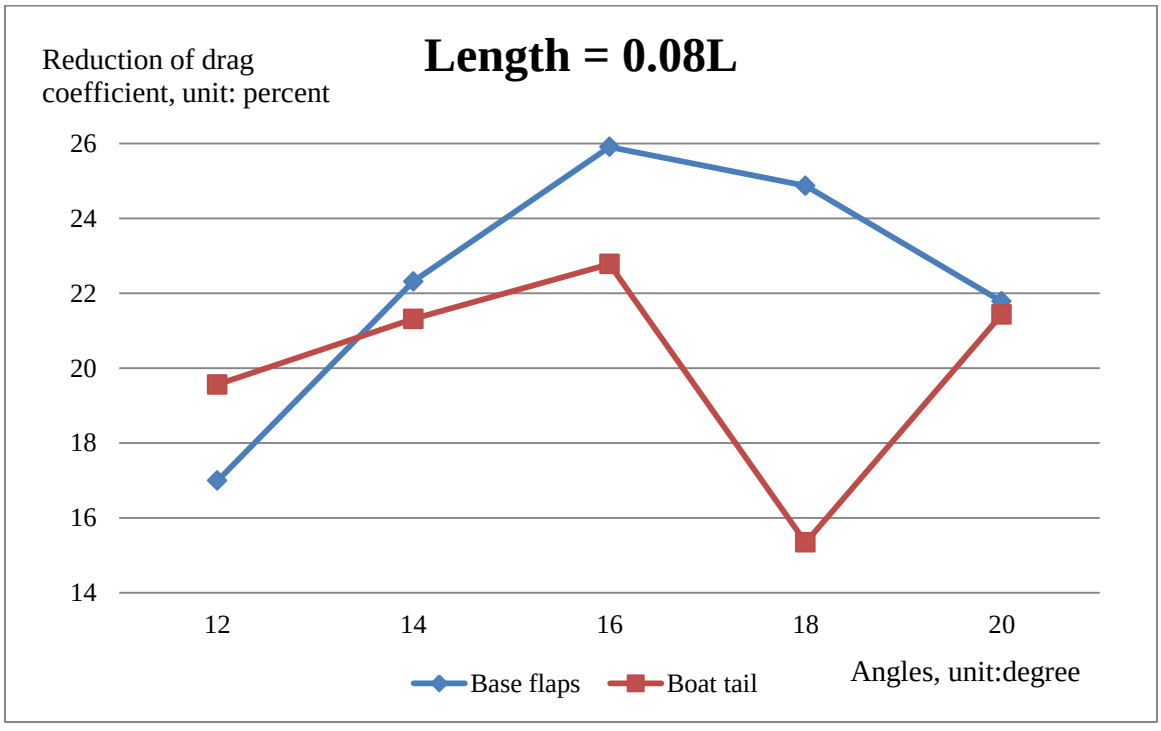

Figure 34. Comparison of the drag reduction, 0.08L, detailed geometry.

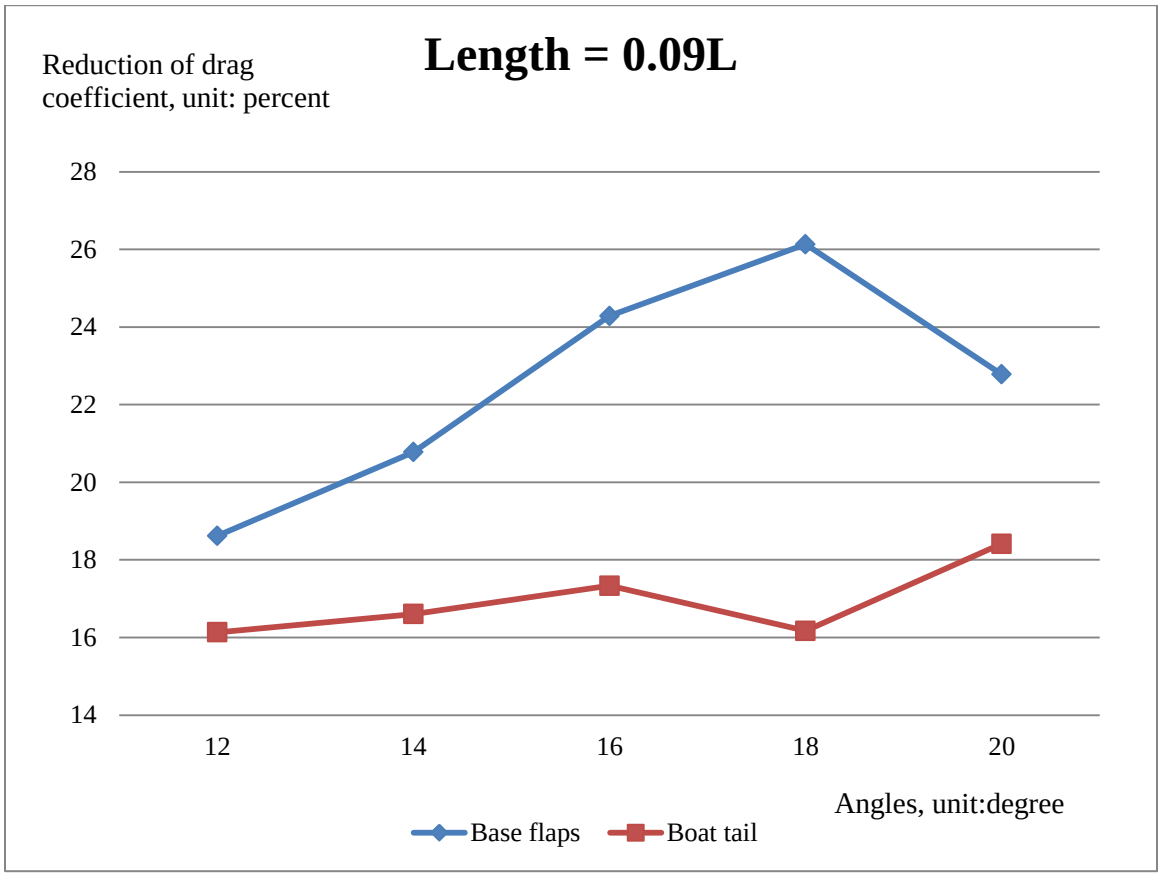

Figure 35. Comparison of the drag reduction, 0.09L, detailed geometry.

5.3.4 Configuration with Multiple Add-on Devices

In order to achieve the maximum drag reduction, baseline geometry was configured with multiple add-on devices. That is, the optimum design of the base flap or boat tail were applied to the baseline geometry, along with the roof cap, underbody skirt and tractor-trailer seal. The result is shown in Table 16. As one can observe, the drag coefficient was reduced significantly when multiple add-on devices were used. However, such high percentage of C_d reduction may not be realized in real world, and further experiments or road tests are required to confirm the trend.

Table 16. Reduction on C_d with Multiply Add-on Devices (Detailed Geometry).

	Baseline	Baseline with skirt, seal and base flaps	Baseline with skirt, seal and boat tail
Mesh Size	5.5M	7.1M	7.1M
C_d	0.579	0.395	0.413
C_d reduction in percentage	N/A	32.789	28.670

5.4 Simulation Modifications

5.4.1 Rotation of the Wheels

In the process of the grid independent study using the detailed truck geometry, simulations were conducted with the application of rotation of the wheels. The results and the comparisons between the rotational and non-rotational wheels for the detailed baseline truck geometry are shown in Table 17. C_d represents the drag coefficient of the baseline geometry without applying the rotation of wheels, while C_d' represents those with rotation. From the comparison, one can observe that the rotation of the wheels increases the drag coefficient a small amount, since the turbulence generated by the wheels increases the pressure difference. However, the differences are negligible. Therefore, the rotation of the wheels was disabled in this study to reduce the computation costs.

Table 17. Comparison between the Simulations with/without Wheel Rotation.

Case	Coarse1	Coarse2	Medium1	Medium2	Fine1	Fine2	Fine3
Size (M)	2.5	3.0	4.0	4.5	5.5	6.0	7.0
C_d	0.612	0.604	0.591	0.583	0.579	0.581	0.580
C_d'	N/A	N/A	0.593	0.586	0.581	0.583	0.582

5.4.2 Setting the Motion of Wall as Translation

As described in Chapter 4, the computational domain was established to be 10 characteristic lengths (10L) upstream, 20L downstream, 10 characteristic widths (10W) to the sides, and about 15 characteristic heights (15H) in height, so that the entire domain could satisfy the free stream condition with zero normal gradients of all flow variables at the sides and top faces. However, if one sets the motion of the wall as translation, given the same velocity as the wind to the wall, the interference will be decreased. Therefore, the reduced volume of the fluid domain will lead to a smaller size of the mesh, causing a decrease in CPU time. As the result, the translation of the wall had been applied in this study.

5.5 Wind Tunnel Validation

In order to validate the results from CFD simulations, a set of experiments were conducted by a team of collaborators at the USTC. Based on the detailed baseline geometry, the truck model was built by the Thirteenth Department of USTC, scaled to 1:20, as shown in Figures 37 to 40.

Table 18. Main Parameters of the Wind Tunnel.

The parameters of wind tunnel	Specific value
Velocity range in the test section	3m/s-50m/s
Turbulence intensity	$\leq 0.08\%$
Dynamic pressure coefficient	$\leq 0.5\%$
Static pressure gradient in bearing	≤ 0.005/m
Space angle avertence of mainstream	$\leq 0.5^0$
Average avertence of mainstream	$\leq 0.2^0$
Stability coefficient of dynamic pressure	≤ 0.005
Noise in test section	$\leq$ 75db at 50m/s

Table 19. Comparison between the Results from Wind Tunnel and CFD Simulations, Both Scaled Models.

Velocity	C_d from wind tunnel experiments	C_d from CFD simulations
19.50m/s	0.5821	0.5782
22.19m/s	0.5830	0.5782
24.96m/s	0.5801	0.5784
27.78m/s	0.5791	0.5782
30.48m/s	0.5761	0.5783

C_d from CFD simulations (1:1 Baseline model, Velocity = 60MPH) = 0.581

The aerodynamic drag experiments were carried out in the wind tunnel at USTC. The test section of the wind tunnel was a square $1000 \times 1000\ \mathrm{mm}^2$ cross section. The force transducer balance installed in the test section synchronously recorded six components of forces and moments, with a measurement accuracy of ± 1Pa. The main

parameters of the wind tunnel used are outlined in Table 18. The comparison between the results from the wind tunnel experiments and the CFD simulations are shown in Table 19.

The difference between the results from the wind tunnel itself was due to the difference of the viscous force, which is a dependent factor of the Reynolds number that changes along with the variation of the velocity. Despite this factor, one can find the difference between the CFD simulation and wind tunnel experiment is not significant, as low as 0.7%, which could be considered negligible. Moreover, a set of CFD simulations were conducted with scaled baseline geometry, which has the same size as the truck model in the wind tunnel experiments; as shown in Table 19, the results also showed similar results. Therefore, the physics models and the meshes used in this CFD simulation can be considered validated.

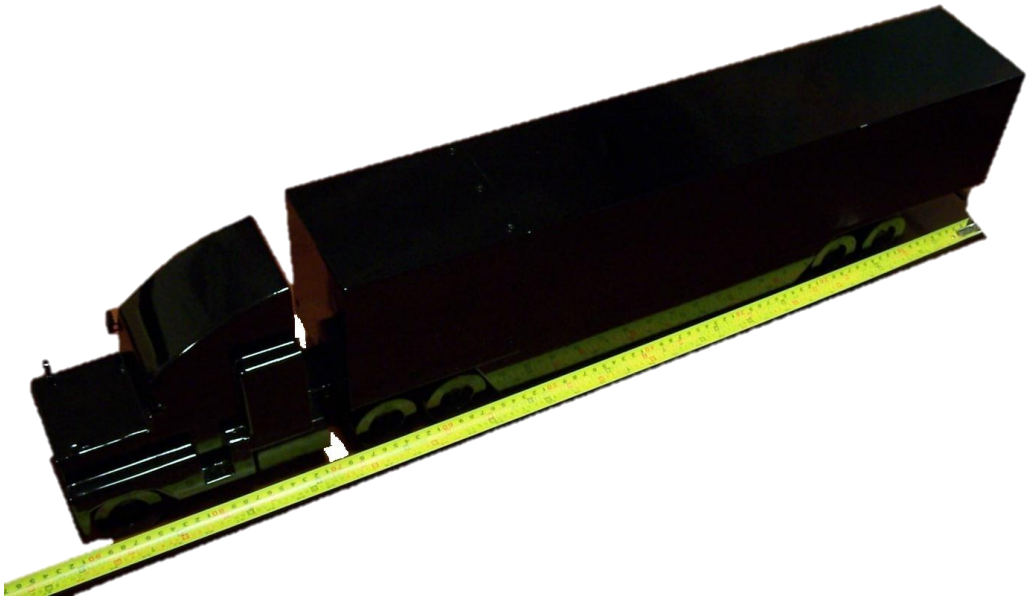

Figure 36. The truck model used in wind tunnel experiments, total length is 900mm. *(Courtesy of Dr. Wang, USTC, China)*

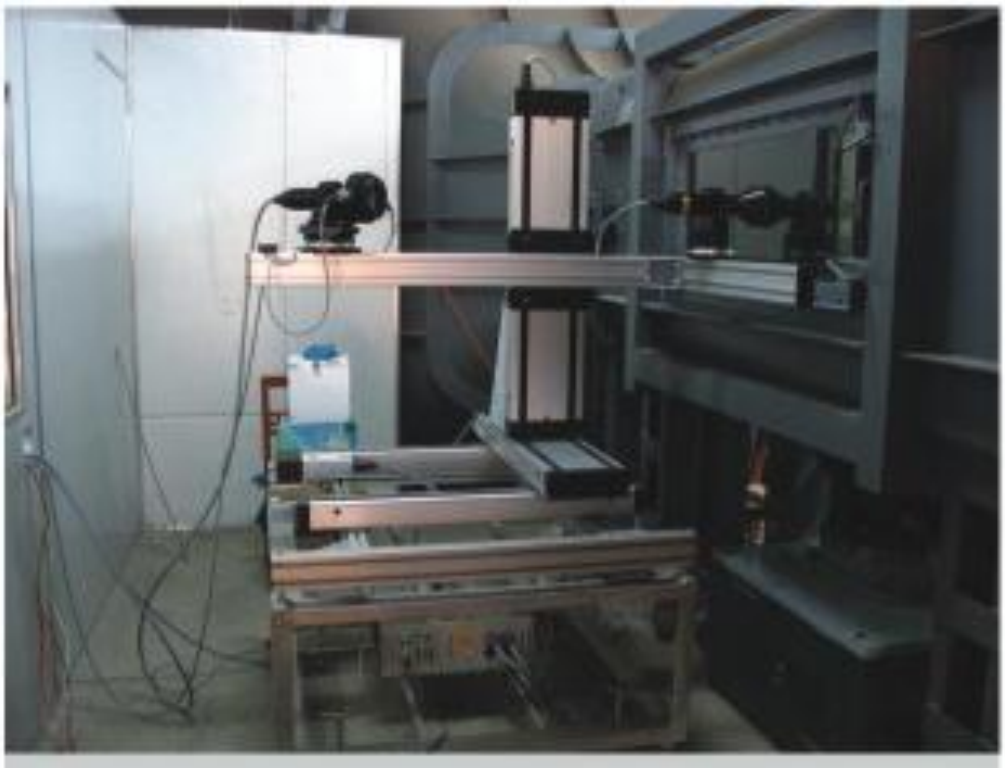

Figure 37. The wind tunnel used in the experiments. *(Courtesy of Dr. Wang, USTC, China)*

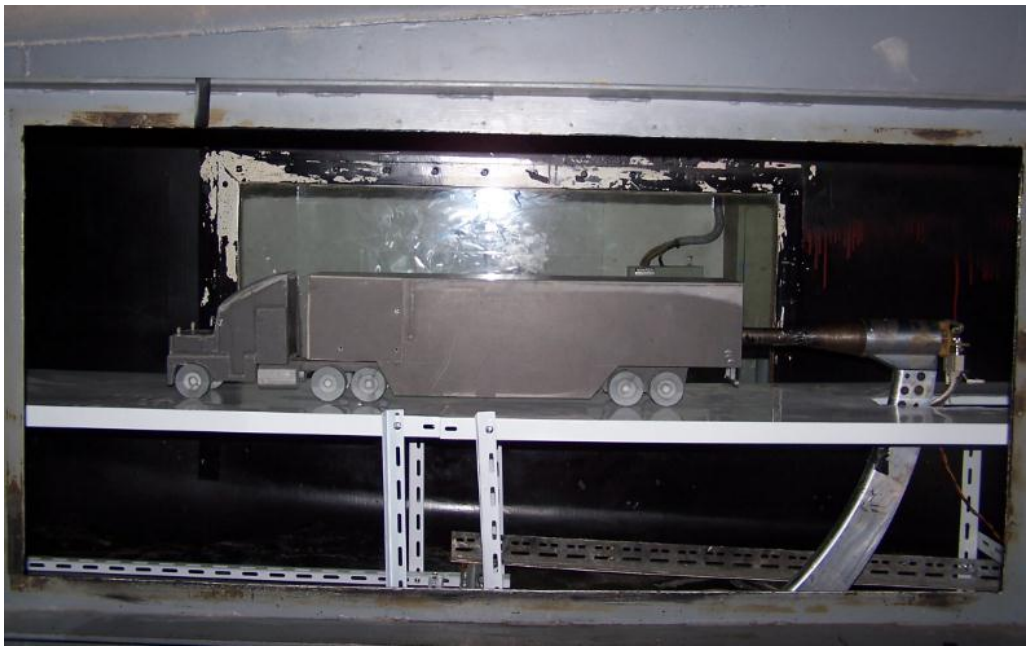

Figure 39. Truck model in the wind tunnel, with underbody skirt. *(Courtesy of Dr. Wang, USTC, China)*

Figure 40. Truck model in the wind tunnel, after level configuration of the ground. *(Courtesy of Dr. Wang, USTC, China)*

CHAPTER 6

SUMMARY & CONCLUSION

Computational fluid dynamics is a well-established engineering discipline in the study of vehicle aerodynamics. Because of its main benefits of lower cost compared with wind tunnel tests and ability to provide a more detailed flow field, CFD software is playing a profound role in aerodynamics studies today.

In this CFD-based study of Class 8 heavy truck drag reduction, a simplified and a detailed truck geometry were designed from scratch using a CAD software. Their dimensions are in compliance with Department of Transportation specifications. Their corresponding add-on devices, including base flap, boat tail, underbody skirt, and tractor-trailer seal, were also created for this study. All of these geometries were used with the CFD software to examine the C_d and the effect of drag coefficient reduction with the use of add-on devices. In order to reach the maximum reduction of the drag coefficient, a parametric study using CFD simulations with different configurations of the add-on devices was conducted. As the result, a better design of the base flap that could provide a drag reduction as high as 28.497% was identified.

In order to validate the results from the CFD simulations, a scaled truck model (1:20) was created at USTC for the wind tunnel experiments. Even though the wind tunnel experiments did not cover all of the configuration combinations used in the CFD simulations, key configurations were studied in the wind tunnel. A comparison between

the results from CFD simulations and wind tunnel experiments demonstrated that the results agreed relatively well, and therefore, the CFD simulations can be considered valid. In conclusion,

- High qualities meshes were generated in this study for both simplified and detailed geometry, with a grid independent study to identify the mesh size for use in this study.
- SST $k-\omega$ model presents a better numerical stability in the vehicle's aerodynamics study than the $k-\epsilon$ model.
- C_d values can be decreased by reducing the vortices in the flow field.
- Both the simplified and detailed geometry simulations indicated the base flap design has a better effect on the drag coefficient reduction than the boat tail design.
- The drag coefficient reduction of the base flaps can reach as much as 28.5%, higher than the boat tail design. However, wind tunnel experiments and road tests are still needed to further validate this finding.
- The drag coefficient reduction of the vehicle with all add-on devices can potentially achieve 32.8% from the CFD simulation. Despite that this outcome was not verified with wind tunnel experiments or road tests, it does indicate a promising trend.

Therefore, add-on devices for the class 8 trucks can be practical and effective solutions to improve their fuel efficiency. As a result, not only that transportation costs can be reduced, it can also help to reduce the emission of air pollutants and the greenhouse gas.

LIST OF REFERENCES

1. "Research and Innovative Technology Administration," National Transportation Statistics, U.S. Department of Transportation, Washington D.C., 2011. Available at, http://fastlane.dot.gov/2011/08/cafe-trucks.html

2. "EPA and NHTSA Propose First-Ever Program to Reduce Greenhouse Gas Emissions and Improve Fuel Efficiency of Medium- and Heavy-Duty Vehicles: Regulatory Announcement." Office of Transportation and Air Quality, October 2010. Available at, http://www.nhtsa.gov/staticfiles/rulemaking/pdf/cafe/CAFE_2014-18_Trucks_FactSheet-v1.pdf

3. "Fuel Standards for Heavy Vehicles," Washington D.C., July 2011. Available at, http://www.doe.gov/articles/doe-announces-293-million-projects-research-development-and-demonstration-alternative

4. "Obama Administration Launches Cost-saving Fuel-efficiency Standards for Trucks." Available at, http://www.bizjournals.com/jacksonville/news/2012/04/23/fuel-efficiency-standards-to-save.html

5. McCallen R, "DOE's effort to reduce truck aerodynamic drag through joint experiments and computations," April 2006.

6. Franzese O, Knee H.E., Slezak L., "Effect of tires on Class 8 heavy truck fuel efficiency." Available at, http://info.ornl.gov/sites/publications/files/Pub20686.pdf

7. Mohamed-Kassin Z., Filippone A., "Fuel Savings on a Heavy Vehicle via Aerodynamic Drag Reduction," *Journal of transportation research.* 2010. (15), 275-284.

8. "New Funding Boosts Carbon Capture, Solar Energy and High Gas Mileage Cars and Trucks." Available at, http://www.doe.gov/articles/new-funding-boosts-carbon-capture-solar-energy-and-high-gas-mileage-cars-and-trucks

9. Hyams D.G., Screenivas K., Pankajakshan R., Nichols D.S., Briley. W.R., and Whitfield D.L., "Computational Simulation of Model and Full Scale Class 8 Trucks with Drag Reduction Devices," *Journal of computers & fluids.* 2011. (41), 27-40.

10. Starccm+ Tutorial Guide, CD-Adapco, 2011.

11. Keye S., "Fluid-structure Coupled Analysis of a Transport Aircraft and Flight-test Validation," *Journal of aircraft.* 2011, Vol48, No.2

12. Finnemore E.J, Franzini J., "Fluid Mechanics with Engineering Applications," *China Machine Press*. Feb, 2006. ISBN 7-111-17723-1.

13. Morgan K., Harlan D., Hassan O., Sorensen K., and Weatherill N., "Steady Incompressible Inviscid and Viscous Flow Simulation Using Unstructured Tetrahedral Meshes. Numerical Simulations of Incompressible Flows," *World scientific Publishing Co. Pte. Ltd*. ISBN 981-238-317-4. Available at: http://ebooks.worldscinet.com/ISBN/9789812796837/9789812796837_0012.html

14. Ito, Y., Shih, A. M. and Soni, B. K., "Unstructured Mesh Generation Using MEGG3D - Mixed-Element Grid Generator in Three Dimensions," *Proceedings of the International Conference on Numerical Geometry, Grid Generation and Scientific Computing (NUMGRID2008),* Moscow, Russia, June 2008, pp. 5-11.

15. Koomullil, R. P., Soni, B.K., and Singh, R.K., "A Comprehensive Generalized Mesh System for CFD Applications," *Mathematics and Computers in Simulation*, Vol. 78, Issues 5-6, pp. 605–617, Sept. 2008.

16. Sazonov, I., Hassan, O., Morgan K. and Weatherill, N.P., "Yee's Scheme for the Integration of Maxwell's Equation on Unstructured meshes," *European Conference on Computational Fluid Dynamics (ECCOMAS CFD 2006)*, the Netherlands, 2006.

17. Aftosmis M.J., Berger, M.J., and Melton, J.E., "Robust and Efficient Cartesian Mesh Generation for Component-Based Geometry." Available at, http://people.nas.nasa.gov/aftosmis/publications/AIAA-97-0196.pdf

18. Skaperdas E., Kolovos C., "Etude in CFD pre-processing," *Proc. of the 7th MIRA International Vehicle Aerodynamics Conference*, Session 7b, Oct.2008.

19. Regert T., Lajos T., "Investigation of Simple Possibilities for Reduction of Drag due to the Wheels of Road Vehicles," *Proc. of 4th European Automotive Simulation Conference*, July 2009.

20. Lombardi G., Maganzi M., Cannizzo F., Cardile E., "Optimization Procedure in a Car Aerodynamic Design: Examples of Application with CFD," *Proc. of the 7th MIRA International Vehicle Aerodynamics Conference*. Oct. 2008, 262-274.

21. Ha J., Jeong S., and Obayasshi S., "Drag Reduction of a Pickup Truck by Rear Downward Flap," *International Journal of Automotive Technology*, Vol. 12, No. 3, pp. 369−374 (2011).

22. Munson, B.R., Young D.F., and Okiishi, T.H., "Fundamentals of Fluid Mechanics," *John Wiley & Sons, Inc*. 1990. ISBN 0-471-85526-X.

23. Spogis N., and Nunhez J.R., "Design of a High-efficiency Hydrofoil Through the Use of Computational Fluid Dynamics and Multiobjective Optimization," *Wiley InterScience*. May14, 2009.

24. Lombardi G., Maganzi M., Cannizzo F., and Cardile E., "Use of the CFD for the Aerodynamic Optimization of the Car Shape: Problems and Application," The *4th European automotive simulation Conference*. July, 2009.

25. Salari K., and Ortega J., "Tractor-trailer Truck Aerodynamics," *Access Science, McGraw-Hill Companies*, 2010.

26. Zhang P., Wang J., and Tang Q., "Experimental Investigation on the Aft-body Drag Reduction of the Tractor-trailer Truck by Aerodynamic Add On Device," *Journal of Experiments in Fluid Mechanics*. Sep 2009, Vol.23, No.3.

27. Crossley W.A., Skillen M.D., Frommer J.B., and Roth B.D., "Morphing Aircraft Sizing using Design Optimization," *Journal of Aircraft*. March-April 2011. Vol.48, No.2.

28. Sahiti N., Durst F., and Geremia P., "Selection and Optimization of Pin Cross-section for Electronics Cooling," *Applied thermal engineering*. 2007, 27, 111-110.

29. Benini E., Ponza R., and Massaro A., "High-life Multi Element Airfoil Shape and Setting Optimization using Multi-objective Evolutionary Algorithms," *Journal of Aircraft*. March-April 2011. Vol.48, No.2.

30. Qi X., and Liu Z., "Investigation on Drag Reduction of Trucks," *Journal of Shanghai Jiaotong University*. 2008, 13(2), 201-205.

31. Al-Garni A.M., and Bernal L.P., "Experimental Study of a Pickup Truck near Wake," *Journal of Wind Engineering and Industrial Aerodynamics*. 2010, 98, 100-112.

32. Shih, A. M., Gopalsamy, S., Ito, Y., Ross, D. H., Dillavou, M. and Soni, B. K., "Automatic and Parametric Mesh Generation Approach," *Proceedings of the 17th International Association for Mathematics and Computers in Simulation (IMACS) World Congress*, Paris, France, July 2005 (CD-ROM)

33. Wu Z., Wei Q., Seizo K., Yohei T., Takashi M., and Kenta Y., "Experimental Study on Reducing Large Bluff-based Vehicles' Drag by using Guide Vances," *ACTA AERODYNAMICA SINICA*. Vol.21, No.4. Dec., 2003.

34. Ma J., Jia Q., and Yang Z., "Method of Selecting High-speed Train Scale Model for Wind Tunnel Testing of Aerodynamic Drag Based on Numerical Computation," *Computer Aided Engineering*. Vol.16, No.3, Sept. 2007.

35. Cai G., "An Experimental Research on Aerodynamic Characteristics of the High-speed Passenger Train Model," *Journal of Experiments in Fluid Mechanics*. Vol.21, No.4, Dec., 2007.

36. Wang F. "The analysis of Computational Fluid Dynamics," *Tsinghua University*. Sept 2004. ISBN 7-302-09503-5

37. Shih, T.-H., Liou, W.W., Shabbir, A., Yang, Z. and Zhu, J. "A New $k-\epsilon$ Eddy Viscosity Model for High Reynolds Number Turbulent Flows -- Model Development and Validation," NASA TM 106721, 1994.

38. Menter, F.R., "Two-equation Eddy-viscosity Turbulence Modeling for Engineering Applications," *AIAA Journal* 32(8) pp. 1598-1605, 1994.

39. Pankajakshan, R., Sreenivas K., Mitchell B., and Whitfield D.L., "CFD Simulations of Class 8 Trucks," 2007-01-4293, SAE 2007 Commercial Vehicle Engineering Congress & Exhibition, October 2007.

40. Pankajakshan, R., Mitchell, B. and Whitfield, D.L, "Full-Scale Simulations of Drag Reduction Devices for Class 8 Trucks," In The Aerodynamics of Heavy Vehicles II: Trucks, Buses, and Trains. *Lecture Notes in Applied and Computational Mechanics.* Springer Berlin/Heidelberg, pp. 339-348. 2009.

41. Sreenivas, K., Mitchell, B., Nichols, III, D.S., Hyams, D.G., and Whitfield, D.L., "Computational Simulation of the GCM Tractor-Trailer Configuration," Aerodynamics of Heavy Vehicles II: Trucks, Buses, and Trains, Lake Tahoe, August 2007.

42. Thompson, J.F., Warsi, Z.U.A., and Mastin, C.W., "Numerical Grid Generation: Foundations and Applications," North-Holland, 1985, ISBN 978-0-521-79309-4.